Accelerated cranial divergence in isolated *Ammospermophilus* lineages: integrating phylogenetic, allometric, and environmental drivers of morphological evolution

Bader H. Alhajeri[1]

[1]Department of Biological Sciences, Kuwait University, Safat, 13060, Kuwait

A - Research concept and design, B - Collection and/or assembly of data, C - Data analysis and interpretation, D - Writing the article, E - Critical revision of the article, F - Final approval of the article

Bader H. Alhajeri - 0000-0002-4071-0301

Abstract:

Understanding what drives morphological variation is important for both evolutionary biology and conservation. This study explores the factors influencing cranial size and shape variation in antelope ground squirrels (genus *Ammospermophilus*) by combining phylogenetic, allometric, ecological, and geographic perspectives. Geometric morphometric analyses were conducted on 58 cranial landmarks from 157 adult specimens representing four species (seven taxa) from 75 localities. Results show that species identity explains more cranial shape variation than allometry. However, after allometric correction, interspecific shape differences become nonsignificant, suggesting that species distinctions are mainly expressed through allometric effects. Ventral cranial shape shows a greater phylogenetic congruence and better distinguishes taxa (80% classification accuracy) than dorsal shape (66%), suggesting different evolutionary pressures across these cranial regions. Temperature, precipitation, and their seasonality explain >60% of environmental variation across species ranges, with *Ammospermophilus leucurus* uniquely exhibiting strong climate–shape covariation (r-PLS: 0.773-0.802). Geographically isolated taxa show increased morphological differentiation, with the insular *A. l. insularis* and peripheral *A. nelsoni* displaying the most divergent cranial morphologies. These results show that antelope squirrels' cranial evolution is shaped by phylogeny, allometry, ecology, and geographic isolation. The marked morphological and genetic divergence of *A. l. insularis* and *A. nelsoni*, along with their limited ranges, and threatened status, makes them key conservation targets for maintaining phylogenetic diversity in this genus.

Keywords: Sciuridae, Climate, Skull, Geometric morphometrics, Allometry, *Ammospermophilus insularis*.

Received: 2025-05-09
Revised: 2026-02-09
Accepted: 2026-02-09
Final review: 2026-02-02

Short title
Ammospermophilus cranial variation

Corresponding author
Bader H. Alhajeri (bader.alhajeri@ku.edu.kw)

Abstract

Understanding what drives morphological variation is important for both evolutionary biology and conservation. This study explores the factors influencing cranial size and shape variation in antelope ground squirrels (genus *Ammospermophilus*) by combining phylogenetic, allometric, ecological, and geographic perspectives. Geometric morphometric analyses were conducted on 58 cranial landmarks from 157 adult specimens representing four species (seven taxa) from 75 localities. Results show that species identity explains more cranial shape variation than allometry. However, after allometric correction, interspecific shape differences become nonsignificant, suggesting that species distinctions are mainly expressed through allometric effects. Ventral cranial shape shows a greater phylogenetic congruence and better distinguishes taxa (80% classification accuracy) than dorsal shape (66%), suggesting different evolutionary pressures across these cranial regions. Temperature, precipitation, and their seasonality explain >60% of environmental variation across species ranges, with *Ammospermophilus leucurus* uniquely exhibiting strong climate–shape covariation (r-PLS: 0.773-0.802). Geographically isolated taxa show increased morphological differentiation, with the insular *A. l. insularis* and peripheral *A. nelsoni* displaying the most divergent cranial morphologies. These results show that antelope squirrels' cranial evolution is shaped by phylogeny, allometry, ecology, and geographic isolation. The marked morphological and genetic divergence of *A. l. insularis* and *A. nelsoni*, along with their limited ranges, and threatened status, makes them key conservation targets for maintaining phylogenetic diversity in this genus.

Keywords

Allometry, *Ammospermophilus insularis*, Climate, Geometric morphometrics, Sciuridae, Skull

Introduction

The genus *Ammospermophilus* Merriam, 1892 (antelope ground squirrels) comprises species named for their affinity to sandy habitats and seed diets (Best et al., 1990c). These rodents inhabit sparsely vegetated arid landscapes such as mountain slopes and sandy regions, where they shelter in self-excavated burrows (Nowak and Paradiso, 1983). Across North America, species cluster in distinct desert regions and exhibit markedly different range sizes, reflecting ecological and geographic divergence (Bowers et al., 2007; Ceballos, 2014). The most widespread species, *A. leucurus*, occupies open shrubby areas with thin soil across the Great Basin, Mojave Desert, and Baja California (Bowers et al., 2007). At the other extreme, *A. insularis* has the narrowest range, being restricted to sandy scrub on Espiritu Santo and Partida islands off Baja California Sur (Ceballos, 2014). The remaining species are of intermediate range: *A. nelsoni* in shrublands and grasslands south of California's San Joaquin Valley, *A. interpres* in rocky Chihuahuan Desert regions, and *A. harrisii* on the plains and valleys of the Sonoran Desert (Bowers et al., 2007; Ceballos, 2014). This ecogeographic diversity—in habitat type, range size, and isolation (insular to widespread)—offers an ideal framework to test drivers of cranial evolution in antelope ground squirrels.

Ammospermophilus contains four (Mammal Diversity Database, 2025), five (McLean et al., 2018; Wilson and Reeder, 2005), or six (Mantooth et al., 2013) species (Fig. 1), with taxonomic sources disagreeing on whether *A. leucurus* represents a single species or should be split into two or three distinct cryptic species. Specifically, *A. insularis* is classified either as a subspecies of *A. leucurus* (e.g., Álvarez-Castañeda, 2007; Mammal Diversity Database, 2025) or as a separate species (e.g., Howell, 1938; Mantooth et al., 2013; Wilson and Reeder, 2005), with Mantooth *et al.* also suggesting the existence of additional cryptic species within the *A. leucurus* complex. Two recent molecular trees (Mantooth et al., 2013; McLean et al., 2018) (Fig. 1) agree that *A. nelsoni*, *A. harrisii*, and *A. leucurus* (excluding *A. insularis*) form a clade (hereafter 'main clade'), but differ on other phylogenetic relationships. Mantooth *et al.* (2013) identified an unresolved trichotomy involving the main clade, *A. interpres*, and a third clade (*A. insularis* + *A. leucurus* from southern Baja California), with *A. leucurus* in the main clade restricted to populations from northern Baja California and the USA. On the other hand, McLean *et al.* (2018) place *A. interpres* sister to the main clade and *A. insularis* as basal. They further disagree on intraclade affinities: Mantooth *et al.* pair *A. leucurus* with *A. harrisii*, whereas McLean *et al.* recover it as sister to *A. nelsoni* (Fig. 1). In *Ammospermophilus*, as in other rodents, phenotypic traits (particularly skull morphology) have traditionally served for species diagnosis (Howell, 1938), yet the correspondence between cranial morphology and molecular phylogenetic relationships remains largely unexplored.

Past research on *Ammospermophilus* cranial morphology has been mostly taxonomic and qualitative (Belk and Smith, 1991; Best et al., 1990d, 1990b, 1990a, 1990c; Howell, 1938). Broader studies on Sciuridae occasionally include *Ammospermophilus* specimens (e.g., McLean et al., 2018), but none specifically examine the predictors of skull variation within this genus. Therefore, a comprehensive quantitative analysis of cranial variation in antelope squirrels is needed to disentangle its phylogenetic, allometric, ecological, and geographic drivers.

Phylogeny and allometry are well studied drivers of mammalian cranial variation, with morphology being constrained by shared ancestry and predictable size-dependent shape changes (Mitchell et al., 2024). In desert rodents specifically, previous work revealed significant phylogenetic signal and allometric scaling patterns in cranial shape, though their relative influence varies across different taxa (Alhajeri, 2025a, e.g., 2025b; Alhajeri and Steppan, 2025).

‘Craniofacial evolutionary allometry’ (CREA) describes a common pattern in mammals where larger body size typically corresponds to a longer face (Cardini, 2019). Recently, this allometric trend has been generalized to include increased skull “gracilization” in larger animals, which is often linked to ecological pressures involving bite force and diet (Mitchell et al., 2024). Both allometric patterns exhibit relatively smaller braincases in larger crania, following Haller’s Rule, where larger species within a clade possess proportionally smaller brains (Rensch, 1948). *Ammospermophilus* cranial allometry remains understudied, leaving its role in shaping skull morphology unclear. Analyzing deviations from expected allometric scaling may reveal key drivers of cranial shape evolution, including developmental constraints, functional adaptations, and ecological specializations (see Mitchell et al., 2024).

Phylogenetic relationships contextualize *Ammospermophilus* cranial diversity, distinguishing ancestral traits from convergent adaptations to environmental pressures. Phylogenetic signal reflects shared ancestry constraining (morphological) trait variation, where strong signal indicates evolutionary conservatism (often via slow neutral drift or stabilizing selection) and weak signal suggests evolutionary lability driven by divergent or convergent selection (see Blomberg et al., 2003; Kamilar and Cooper, 2013). Detecting phylogenetic signal analytically requires sampling at least 20 species for adequate statistical power (Blomberg et al., 2003). The terms “phylogenetic constraint,” “phylogenetic inertia,” or “phylogenetic effect” generally refer to the same pattern (see Blomberg et al., 2003; Kamilar and Cooper, 2013) but without implying statistical testing, making them more appropriate for qualitative assessments of morphological–phylogenetic concordance in smaller clades like antelope squirrels.

While ecological pressures may drive convergent cranial evolution in *Ammospermophilus*, such adaptive hypotheses remain largely untested within this genus. The sole comparative ecological study of antelope squirrels focused on antipredator vocalization–habitat relationships rather than cranial traits (Bolles, 1988). Broader sciurid research links diet, fossoriality, locomotion, and sociality as cranial shape drivers (Bertrand et al., 2021; Cardini and O'Higgins, 2004; Gomes Rodrigues and Damette, 2023; Lu et al., 2014; McLean et al., 2018), while arid-adapted rodents show climate-linked adaptations in the tympanic bullae and nasal passages (e.g., Alhajeri, 2025b; Alhajeri et al., 2025, 2015; Alhajeri and Steppan, 2018). Given *Ammospermophilus*' habitat diversity and demonstrated habitat–skull correlations in other rodents (e.g., Alhajeri, 2025a; Alhajeri et al., 2025; Alhajeri and Steppan, 2025), ecological convergence could uncouple cranial morphology from phylogenetic relationships. The present study addresses the unresolved question of whether cranial variation in antelope squirrels is primarily shaped by phylogenetic history or ecological adaptation.

Geographic isolation, a documented driver of cranial divergence in rodents (e.g., Alhajeri et al., 2025), may similarly shape cranial variation in *Ammospermophilus*, particularly in species with restricted or isolated ranges. Taxa with peripheral (*A. nelsoni*, influenced by "Isolation by Distance") or insular (*A. insularis*, exhibiting "Island Syndrome") distributions experience increased isolation, reducing gene flow and potentially driving cranial divergence through genetic drift and/or local adaptation (see Adler and Levins, 1994; Wright, 1943). Patterns of cranial variation in antelope squirrels may be explained by a combination of these geographic drivers interacting with phylogenetic history and ecological pressures, but the relative influence of each factor remains untested.

The present study investigates cranial shape variation in *Ammospermophilus* through an integrated framework of phylogeny, allometry, ecology, and geography. This variation is quantified via geometric morphometrics, where generalized Procrustes analysis (GPA; Rohlf and

Slice, 1990) removes isometric size to generate shape variables, with allometric effects analyzed separately (see Zelditch et al., 2012). First, I hypothesize that cranial shape aligns with phylogenetic relationships and allometric scaling, predicting morphological similarity among closely related or similarly sized taxa. Second, ecological factors (habitat, climate, diet) are expected to drive cranial convergence among species occupying similar niches, independent of their phylogenetic relatedness. Third, geographic isolation (demonstrated by insular *A. insularis* and peripheral *A. nelsoni*) is predicted to increase cranial divergence through genetic drift and/or local adaptation, consistent with Island Syndrome and Isolation by Distance mechanisms.

Materials and methods

Study taxa

A total of 157 *Ammospermophilus* specimens from all four species were sampled: 50 *A. leucurus* (35 *A. l. leucurus*, 12 *A. l. insularis*, 3 *A. l. cinnamomeus*), 39 *A. nelsoni*, 34 *A. harrisii* (25 *A. h. harrisii*, 9 *A. h. saxicolus*), and 34 *A. interpres* (Appendix 1). The dataset comprises 82 males, 74 females, and one specimen of unknown sex, spanning 75 localities (123 from the United States and 34 from Mexico) (Fig. 2; Data S1). Taxonomy was updated to follow the Mammal Diversity Database (2025), with taxonomic authors detailed in Appendix 1.

Specimens were examined at the American Museum of Natural History (AMNH, New York City), the Field Museum of Natural History (FMNH, Chicago), the Museum of Vertebrate Zoology (MVZ, the University of California, Berkeley), the Florida Museum of Natural History (UF, the University of Florida, Gainesville), and the United States National Museum of Natural History (USNM, Washington, D.C.) (Appendix 1). To minimize the influence of cranial condition and age on the results, only adult crania in the best available condition were selected.

Adult status was determined based on fully erupted cheek teeth and fused parietals, interparietals, and frontals (see Bolles, 1988; Sinitsa et al., 2019).

Locality coordinates were obtained from museum online databases or, when unavailable, determined using Google Maps (Google, 2025) following Alhajeri (2021a) (see Data S1 for details). Localities were mapped in R (R Core Team, 2024) using the rnaturalearth (South, 2017) and ggplot2 (Wickham, 2016) libraries.

Geometric morphometric analysis

Cranial images were captured dorsally and ventrally using a Nikon D3200 digital SLR camera with a 40 mm Micro NIKKOR lens (see Alhajeri, 2019). Each image included 1-mm graph paper for pixel-to-millimeter conversion to estimate centroid size. Using ImageJ (Schneider et al., 2012), 17 dorsal and 41 ventral landmarks were digitized on the left half of each cranium, ensuring even coverage (Fig. 3; Table S1). These landmarks were used in similar rodent studies (Alhajeri et al., 2023; e.g., Alhajeri, 2025b; Alhajeri et al., 2025; Dashti et al., 2022a), excluding those not found in *Ammospermophilus*. For example, standard landmarks like the bregma and lambda are omitted because in most adult *Ammospermophilus* specimens, the interparietals, parietals, and often frontals are completely fused to each other (leaving no visible sutures) forming what resembles a single composite bone (see Bolles, 1988; Sinitsa et al., 2019). In cases where the right half of a cranium was better preserved than the left, I digitally mirrored it across the midsagittal plane before landmark digitization. Only the intact view (e.g., ventral) was digitized if landmarks were missing on the other (e.g., dorsal), yielding complete datasets for geometric morphometric analysis (dorsal: n=149; ventral: n=148) (Data S1).

Landmark coordinates were combined into a single tps file (Rohlf, 2015) and flipped along the y-axis using the function rotate.coords(“flipY”) in the geomorph package (Adams et al., 2024) to match digitization direction (Fig. 3). Generalized Procrustes analysis (GPA; Rohlf and Slice, 1990) was performed with geomorph::gpagen(Proj=T), superimposing landmarks, and projecting them onto tangent space to produce Procrustes shape coordinates and centroid sizes, with the latter log-transformed for further analyses (Data S1). Using geomorph::plotOutliers(), specimens with large Procrustes distances from species’ mean shapes were excluded to minimize effects of cranial condition and digitization errors, reducing the dataset from 170 to 157 specimens after eliminating 13 outliers. All subsequent statistical analyses used nonparametric tests with 999 random permutations (α=0.05).

RRPP-ANOVA and pairwise analysis

Sexual dimorphism in centroid sizes and Procrustes coordinates was tested using the lm.rrpp() function from the RRPP library, which utilizes residual randomization in a permutation procedure (RRPP; Collyer and Adams, 2018). Finding no significant sex effects (see Results), all specimens (males, females, and unknown) were pooled for subsequent analyses.

RRPP models excluding sex treated species as the sole predictor of centroid size, and, for Procrustes coordinates, added centroid size plus its interaction with species to partition shared versus species-specific allometries. F-distribution ANOVA tables were computed for each model, applying hierarchical sums of squares in multifactor Procrustes coordinates analyses to account for unequal sample sizes across species (Langsrud, 2003). Following significant interspecific differences (see Results), RRPP::pairwise() calculated species-pair distances based on mean centroid sizes and Procrustes coordinates (both with and without allometric adjustments), generating pairwise distances, effect sizes, p-values, and confidence limits via RRPP::summary.pairwise(). Intraspecific pairwise tests were similarly performed on the two most heavily sampled subspecies within *A. harrisii* and *A. leucurus*. Finally, I visualized size differences across taxa with ggplot2 boxplots.

Linear discriminant analysis and allometric scaling

I performed a linear discriminant analysis (LDA) to test the ability of Procrustes coordinates to differentiate taxa. Procrustes coordinates were prepared using geomorph::prep.lda() (specifying the taxon as the sole variable), which projects them onto principal components (PCs) for taxon prediction (Collyer and Adams, 2018). The LDA was then performed via the lda() function from the MASS package (Venables and Ripley, 2002) and classification accuracy was assessed through a leave-one-out cross-validated confusion matrix.

Because species-by-centroid-size interactions were significant in the dorsal Procrustes coordinates model (and marginal in the ventral model; see Results), I explored allometry by visualizing shape–size covariation. Standardized shape scores (RegScore; Drake and Klingenberg, 2008) were derived by regressing Procrustes coordinates on centroid sizes, and analyzed for allometry via geomorph::plotAllometry(method="RegScore"). I fitted species-unique allometry models to allow slope heterogeneity and visualized their divergent trajectories using species-specific regression lines. Extreme shapes (minimum/maximum RegScores) were represented as thin-plate spline (TPS) deformation grids using geomorph::plotRefToTarget(), with the sample mean shape (geomorph::mshape()) as reference and the extreme shapes (geomorph::shape.predictor()) as targets. Landmarks were connected using geomorph::define.links() to improve biological interpretability.

Principal component analysis and mean-shape clustering

I performed principal component analysis (PCA) on Procrustes coordinates using geomorph::gm.prcomp() to identify major axes of shape variation, plotted PC1 and PC2 scores, and depicted extreme shapes as TPS deformation grids (mirroring the RegScore analysis).

Taxon-mean shapes were computed using geomorph::mshape() followed by GPA realignment. Taxon-mean clustering patterns were assessed via UPGMA (unweighted pair group method with arithmetic mean) dendrograms (Sneath and Sokal, 1973) derived from Procrustes distance matrices from the realignment, using the base R function hclust(method=“average”). UPGMA was chosen because it yielded consistent and reliable results in prior studies involving other rodent taxa (Alhajeri, 2025a, 2023, e.g., 2021b; Alhajeri and Steppan, 2025). I generated separate dorsal and ventral dendrograms, along with a composite dendrogram based on the equally weighted average of their matrices. I further assessed taxon differentiation by estimating a ‘mean of means’ shape for each view—equally weighting each taxon regardless of sample size (unlike the sample-wide averages in RegScore and PCA—and visualizing each taxon-mean’s deviation from this consensus with TPS deformation grids.

Climatic PCA and two-block partial least squares analysis

Locality climate data were estimated using 19 WorldClim (version 2) bioclimatic variables (Fick and Hijmans, 2017; https://www.worldclim.org/bioclim), downloaded as 2.5-minute raster files using the raster package (Hijmans, 2019). Variables were standardized (zero mean, unit variance) using the base R function scale() to account for unit differences.

A PCA on these standardized variables yielded PC1-2, together capturing 64.4% of climatic variation, which were visualized in scatterplots. Throughout all visualizations (locality map, RegScore, shape and climate PCA plots), species were differentiated by symbols and subspecies by colors.

The relationship between intraspecific cranial variation and climate was assessed using two-block partial least squares (2B-PLS; Rohlf and Corti, 2000) via geomorph::two.b.pls(). This function evaluates relationships between standardized climate variables, and both logged centroid sizes and Procrustes coordinates, analyzing each species separately (not considering subspecies membership).

Results

Components of variation and classification accuracy

No significant sexual dimorphism was detected in centroid size or Procrustes coordinates in either view (all $p>0.050$), justifying the pooling of males, females, and unsexed specimens. This agrees with Best *et al.* (1990c)., who found minimal cranial differences between sexes in *Ammospermophilus* using linear measurements.

In pooled RRPP analyses, centroid size differed significantly among species in both dorsal and ventral views (both $p<0.050$; Z=3.17–4.87; $R^2=0.121–0.878$; Table 1a), and three of six species pairs showed significant pairwise size differences in both views (all $p<0.050$; Z=2.26–3.64; Table 2a). In both dorsal and ventral views, boxplots show *A. nelsoni* as the largest, *A. leucurus* and *A. h. saxicolus* as the smallest, and the remaining taxa intermediate in size (Fig. 4). Notably, conspecific subspecies sometimes differ markedly in size (Fig. 4). Pooled cranial shape models revealed even stronger interspecific differences (both $p<0.050$; Z=7.10–

9.78; R^2=0.118–0.205; Table 1b). Centroid size significantly influenced shape in both views (both $p<0.050$; Z=3.20–4.01; R^2=0.018–0.021; Table 1b), and a size × species interaction (evidence of species-unique allometries) was significant dorsally ($p<0.050$; Z=2.58; R^2=0.031), and marginal ventrally (p=0.057; Z=1.52; R^2=0.021; Table 1b). All six species pairs significantly differed in shape in both views (all $p<0.050$; Z=3.40–6.15; Table 2b), but no pairwise differences remained after accounting for common and unique allometries (all $p>0.050$; Table 2c).

Intraspecifically, *A. h. harrisii* did not significantly differ from *A. h. saxicolus* in size or shape in either view (all $p>0.050$; Table S2). By contrast, *A. l. insularis* was significantly larger than *A. l. leucurus* dorsally ($p<0.050$; Z=2.65; R^2=0.210), but not ventrally ($p>0.050$; Table S2a), and its cranial shape differed in both views (both $p<0.050$; Z=4.81–5.26; R^2=0.177–0.178; Table S2b). Shape LDA classified subspecies more accurately from ventral (80%) than dorsal (66%) data (Table S3). The highest accuracies occurred in monotypic species or those with a single sampled subspecies—*A. interpres* (85–100%) and *A. nelsoni* (79–89%)—and *A. l. insularis* (100% in both views; Table S3). The remaining misclassifications were mainly within species (e.g., *A. h. saxicolus* being misclassified as *A. h. harrisii* and vice versa). Disregarding subspecies and analyzing at the species level increased overall classification accuracy in both views to 71–91%.

Allometric scaling, PCA morphospace, and clustering of mean shapes

TPS deformations at RegScore extremes reveal that increased cranial size is associated with rostral elongation, facial and zygomatic arch expansion, and braincase contraction (Fig. 5). In dorsal view, rostral extension involves the nasals, premaxillae and maxillae, while the occipital region is reduced (Fig. 5a). Ventrally, rostral lengthening mostly involves incisive bones; other modifications include a narrower palatine fissure, an anteriorly shifted masseteric tubercle, an expanded molar row, and narrowed tympanic bullae and foramina magna (Fig. 5b). In both views, *A. leucurus* shows the steepest allometric trajectory and *A. interpres* the flattest (Fig. 5).

PC1–2 captured 30.9% of dorsal and 33.4% of ventral cranial shape variation (Fig. 6). Despite some overlap in morphospace, taxa form distinct clusters and exhibit greater dispersion in the ventral view than in the dorsal view (Fig. 6). In the dorsal plot, PC1 contrasts specimens with elongated rostra, enlarged faces, flared zygomatic arches, and reduced braincases (e.g., *A. nelsoni* and *A. l. leucurus*) near the minimum against those with opposite patterns (e.g., *A. h. saxicolus* and *A. interpres*) near the maximum (Fig. 6a). PC2 differentiates specimens with widened crania, blunted rostra (shorter nasals and premaxillaries), flared zygomatic arches, and compressed braincases near the minimum from those with converse patterns near the maximum (Fig. 6a). This PC2 variation mostly reflects within-taxon variation rather than intertaxonomic divergence. On the ventral PC1, specimens near the minimum (especially *A. nelsoni*) have shortened nasals, elongated incisive bones, expanded molar rows, flared zygomatic arches, and enlarged tympanic bullae, foramina magna magnum, and braincases, along with compressed rostra, while those near the maximum (e.g., *A. l. insularis* and most *A. interpres*) display the opposite suite of traits (Fig. 6b). PC2 contrasts specimens with broad crania with enlarged zygomatic arches and tympanic bullae (e.g., *A. interpres*) near the minimum from those with converse patterns (e.g., *A. h. harrisii* and somewhat *A. h. saxicolus*) near the maximum (Fig. 6b).

Dorsal (Fig. S2a) and ventral (Fig. S2b) shape dendrograms showed different clustering patterns. Because the ventral dendrogram more closely mirrors the phylogenies in Fig. 1, its clustering is reported below in comparison with the two trees. In the ventral dendrogram, *A. l. cinnamomeus* + *A. l. leucurus* and *A. h. harrisii* + *A. h. saxicolus* form separate clusters, which are then joined by *A. nelsoni* (Fig. S2b). These three species form a clade in both phylogenetic trees in Fig. 1. *A. interpres* then joins this main cluster (Fig. S2b). In the first phylogeny, *A. interpres* forms its own branch (Fig. 1a), whereas in the second it joins the main clade (Fig. 1b). *A. l. insularis* is the most distal taxon in the ventral dendrogram (Fig. S2b), forming a separate third lineage in Fig. 1a (alongside an unsampled species) and occupying the basal position in Fig. 1b.

The composite dendrogram (Fig. 7), which integrates dorsal and ventral data, resulted in clustering intermediate to the separate dendrograms (Fig. S2) and shows lower congruence with the phylogenies (Fig. 1), instead reflecting overall cranial shape similarity. In this dendrogram, *A. l. insularis* is the first to diverge, its mean-shape characterized by broad rostra (especially the maxilla), enlarged palatine fissures, distinctive zygomatic arches, the smallest tympanic bullae, and a contracted cranial base (Fig. 7). *A. l. cinnamomeus* splits next, showing among the largest rostra (driven by premaxilla expansion despite reduced nasals); considering sparse sampling in this taxon, these patterns should be confirmed when more suitable samples become available. *A. nelsoni* diverges next, characterized by a broad cranium, enlarged zygomatic arches, and the largest tympanic bullae (Fig. 7). Subsequently, *A. interpres* diverges with broad nasals, unflared zygomatic arches, and elongated occipitals. *A. l. leucurus* splits next, followed by the *A. h. harrisii* + *A. h. saxicolus* cluster; all three exhibit cranial shapes intermediate among the sampled taxa, reflecting the genus-typical morphology (Fig. 7).

Climate-associated morphological variation

Climate accounted for 38% of the variance on PC1 and 25% on PC2 (Fig. 8; Table S4). PC1 represents a temperature gradient, with relatively strong negative loadings on Annual Mean

Temperature (BIO1, –0.34), Minimum Temperature of the Coldest Month (BIO6, –0.32), and Mean Temperature of the Coldest Quarter (BIO11, –0.34), with temperature variability measures showing weaker positive loadings: Temperature Seasonality (BIO4, +0.14) and Annual Temperature Range (BIO7, +0.08; Table S4). Negative PC1 scores thus correspond to warm, climatically stable sites, while positive scores indicate cooler, more seasonal climates (Fig. 8). PC2 represents a precipitation gradient, driven mainly by Precipitation of the Wettest Month (BIO13, +0.39), Precipitation of Wettest Quarter (BIO16, +0.37), and Precipitation Seasonality (BIO15, +0.36), with moderate contributions from Annual Precipitation (BIO12, +0.28) and Precipitation of the Warmest Quarter (BIO18, +0.30; Table S4). Negative PC2 values therefore indicate arid, non-seasonal climates and posotove values represent more mesic conditions with higher variability (Fig. 8).

Most taxa overlap in PC1–PC2 climate space (Fig. 8), indicating broadly shared climatic adaptations, though some diverge. Excluding an extreme PC2 outlier in *A. h. saxicolus*, that subspecies still exhibits the widest niche. Both *A. h. harrisii* and *A. l. cinnamomeus* occupy dry, low-seasonality environments: *A. h. harrisii* in warm regions (lower left quadrant), and *A. l. cinnamomeus* across lower quadrants regardless of temperature (Fig. 8). *A. l. insularis* lies at the opposite extreme (upper left), reflecting warm, wet habitats with high precipitation seasonality but low temperature seasonality. *A. l. leucurus* spans intermediate positions with a slight tendency toward drier, non-seasonal conditions (lower quadrants) (Fig. 8). *A. interpres* occurs in cooler, highly seasonal environments (right quadrants) and *A. nelsoni* appears in moderately warm, low-seasonality climates (intermediate-to-left quadrants) (Fig. 8).

The 2B-PLS analysis showed significant covariation between climate and cranial size in all species in both dorsal and ventral views (all $p<0.050$; $Z=1.92–3.07$; r-PLS=0.392–0.576) except *A. nelsoni* (both p>0.050; Table S5a). By contrast, climate–shape covariation was nonsignificant in all taxa in both views (all p>0.050) except *A. leucurus* (both p<0.050; Z=3.32–4.26; r-PLS=0.773–0.802; Table S5b).

Discussion

Allometric scaling

Species identity accounted for around 6–10 times more cranial shape variation in *Ammospermophilus* than allometry (cf. R^2 in Table 1b), with all six species pairs differing significantly in shape (Table 2b) but only three differing in size (Table 2a). However, when shared and unique allometric components were statistically removed (Table 2c), interspecific cranial shape differences disappeared, a pattern previously reported in other rodents (Alhajeri, 2025a, 2025b, 2021c; Alhajeri et al., 2025; Alhajeri and Steppan, 2025). This suggests that species-specific shape divergence is mainly driven by modifications in allometric scaling trajectories, highlighting allometry's central role in generating interspecific cranial differences (see Marroig and Cheverud, 2005).

Size-related cranial shape changes in *Ammospermophilus* follow an allometric pattern where larger crania show rostral elongation, facial and zygomatic arch expansion, and braincase contraction (Fig. 5). These modifications conform to the aforementioned CREA pattern (Cardini, 2019; Mitchell et al., 2024) and Haller's Rule (Rensch, 1948), and correspond to patterns previously observed in other rodents (Alhajeri, 2025a, 2022, 2021c; Alhajeri and Steppan, 2025; Dashti et al., 2022b; Marcy et al., 2020). Furthermore, these size-related cranial shape changes (Fig. 5) align almost exactly with PC1 of dorsal variation (Fig. 6a), indicating that allometric changes drive the main axis of cranial shape variation in antelope squirrels.

Differences in allometric slopes among *Ammospermophilus* species likely reflect either lineage-specific developmental constraints or adaptive responses to divergent ecological pressures, which together influence how cranial shape scales with size (see Marcy et al., 2020; Wilson, 2013). Species-specific and shared allometric trajectories each explained ~2–3% of cranial shape variation (Table 1b), with *A. leucurus* exhibiting the steepest slope and *A. interpres* the shallowest, while *A. harrisii* and *A. nelsoni*'s slopes were intermediate (Fig. 5). These slope differences may reflect functional adaptations to feeding mechanics, since rostrum elongation and zygomatic arch expansion (Fig. 5) are features that reduce mechanical stress during feeding in rodents and correlate with bite force variation and niche divergence (Cox et al., 2012; Maestri et al., 2016). Even minor divergences in allometric trajectories, such as those observed here, may facilitate divergent functional specialization (e.g., see Tavares et al., 2019), highlighting allometry's role in driving cranial diversity within antelope squirrels.

Phylogenetic congruence

The ventral cranial shape of *Ammospermophilus* exhibits a stronger phylogenetic effect (i.e., aligns more closely with molecular phylogenies) than its dorsal shape (Figs. 1, 6, 7, S2), suggesting differential evolutionary constraints across cranial regions. Ventral PCA (Fig. 6b) reveals broader morphospace dispersion and clearer taxonomic clustering (despite some overlap) than the dorsal PCA (Fig. 6a). This superior discrimination likely reflects the taxonomic value of ventral structures, including the auditory bullae, toothrows, and zygomatic arches, which previous work in sciurids has shown to carry strong phylogenetic effect (Álvarez-Castañeda, 2007; Belk and Smith, 1991; Lu et al., 2014). Early taxonomic work on antelope squirrels relied on size and pelage coloration (Howell, 1938), while later studies showed ventral cranial features (e.g., auditory bullae, occipitals, zygomatic arches, dental traits) provide more reliable taxonomic markers (Belk and Smith, 1991; Best et al., 1990b, 1990d; Cox et al., 2012). Ventral PC1 clearly separates *A. nelsoni* (characterized by compressed rostra, shorter nasals, elongated incisive bones, flared zygomatic arches, larger molars, and enlarged tympanic bullae and foramina magna) from *A. l. insularis* and *A. interpres* (Fig. 6b), reflecting both deep evolutionary divergence and distinct ecological adaptation. The three principal lineages in this genus that Mantooth *et al.* (2013) identified (Fig. 1a) split during the Miocene–Pliocene desert formation—a division mirrored in the ventral taxon-mean shape clusters (Fig. S2b). Together with Miocene fossil records documenting *Ammospermophilus*' early origins (Belk and Smith, 1991), these results highlight the value of ventral cranial morphology for resolving both the evolutionary history and ecological diversification in this genus.

Dorsal PC2—separating wider crania with blunt rostra, flared zygomatics, and compressed braincases from crania with opposite features (Fig. 6a)—primarily reflects intrataxonomic differences, suggesting lower phylogenetic inertia in dorsal regions. The LDA revealed that ventral cranial shape provides better taxonomic discrimination than dorsal shape (80% vs. 66% classification accuracy), with accuracy improving to 71-91% when analyzed at the species, rather than subspecies, level (Table S3). The difference in phylogenetic congruence between dorsal and ventral views aligns with findings in other rodents: dorsal cranial regions typically respond more readily to ecological pressures (habitat use, feeding behavior), while ventral structures (zygomatic arch, auditory bulla, dentition) remain more developmentally constrained and phylogenetically conserved, though still reflecting some dietary adaptations (Cox et al., 2012; Lu et al., 2014; Maestri et al., 2016; McLean et al., 2018). This suggests ventral cranial features provide more reliable phylogenetic information and should be prioritized in taxonomic and systematic studies of *Ammospermophilus* and possibly other squirrels.

Phenotypic clustering of skeletal and vocal traits in *Ammospermophilus* sometimes conflicts with molecular phylogenies, suggesting habitat-driven selection can mask true evolutionary relationships (see Best et al., 1990c, 1990a; Bolles, 1988; Ceballos, 2014; Hafner et al., 1998). That ventral cranial shape clustering (Fig. S2b) mirrors molecular phylogenies (Fig. 1), while dorsal shape (Fig. S2a) shows weaker concordance, implies that these regions have responded to distinct ecological or developmental pressures and thus warrant separate analyses.

Functional demands can override phylogenetic constraint in certain cranial regions. For example, Cox *et al.* (2012) document repeated parallel adaptations in craniomandibular muscle morphology linked to feeding specialization overpowering phylogenetic history, and Mitchell *et al.* (2024) show that strong phylogenetic signal in overall cranial size can mask underlying evolutionary allometry. These cases show that diet-related and size-related pressures may shape crania independently of shared ancestry. Broad comparative studies in Sciuridae show that while phylogeny and allometry set baseline constraints on craniodental morphology, adaptive shape changes in particular lineages and skull regions often diverge from phylogenetic expectations, with the relative influence of phylogenetic, allometric, and ecological drivers varying among clades and regions (see Lu et al., 2014; McLean et al., 2018; Menéndez et al., 2023).

Ecological drivers

Considering that temperature and precipitation gradients explain >60% of climatic variation across *Ammospermophilus* (Fig. 8), climate is a likely driver of its cranial morphological diversity. PC1 describes a continuum from warm, stable to cool, variable climates, while PC2 ranges from dry, consistent to wet, seasonal conditions (Table S4). This climatic framework allows assessing how environmental pressures shape cranial morphology in this genus, since similar temperature and precipitation gradients correlate with cranial variation in other desert-adapted rodents (Alhajeri et al., 2015; Alhajeri and Steppan, 2018).

Geographic variation in body size is a common pattern in several *Ammospermophilus* species (Best et al., 1990c; Ceballos, 2014). This variation often appears as larger size in cooler regions, and lighter pelage (and often enlarged bullae) in more arid regions, indicating that such environmental gradients play a significant role in shaping morphological traits (Belk and Smith, 1991; Best et al., 1990b, 1990d). The 2B-PLS analysis confirmed a significant association between climate and cranial size in all species except *A. nelsoni* (Table S5a). This prevalent climate-size trend point to consistent selective pressures (e.g., thermoregulation, resource availability) on morphological variation across *Ammospermophilus* species, as previously observed in other rodents (i.e., “Bergmann’s rule”) (Alhajeri and Steppan, 2016; Fourcade and Alhajeri, 2023). The exception of *A. nelsoni* indicates that species-specific factors can override climatic influences on skull size. Combined with earlier evidence of geographic body size clines in *Ammospermophilus* (Best et al., 1990c; Ceballos, 2014), these findings reinforce environmental gradients as drivers of morphological variation in antelope squirrels.

Among *Ammospermophilus* species, only *A. leucurus* exhibited significant covariation between climatic variables and cranial shape, with high r-PLS values (0.773–0.802; Table S5b). As the genus’ most geographically widespread taxon, *A. leucurus* inhabits environmentally heterogeneous regions that expose it to substantial climatic variation (Belk and Smith, 1991; Mantooth et al., 2013), likely driving its increased morphological variability along temperature and precipitation clines. Environmental variation may shape cranial traits via local adaptation, while subspecies diversity, including the potentially distinct *A. l. insularis*, increases genetic and ecological complexity within the species. These findings suggest that widespread taxa with intraspecific phylogeographic structure may develop stronger climate–shape relationships than those with narrower distributions.

Closely related *Ammospermophilus* species often retain similar ecological and morphological traits—a pattern called phylogenetic niche conservatism that may reflect underlying evolutionary constraints (Blomberg et al., 2003; Kamilar and Cooper, 2013; Mitchell et al., 2024). Although they differ in cranial shape (Fig. 7), the largely overlapping climatic niches of most species (Fig. 8) imply shared ecological tolerances. However, some taxa differ sharply in climate: *A. h. harrisii* and *A. l. cinnamomeus* inhabit dry, stable environments, while *A. interpres* inhabits cooler, seasonally variable habitats (Fig. 8). These climatic differences align with the varied habitats of antelope squirrels—from open rocky areas to juniper woodlands—with some species exhibiting ecological flexibility, while others specialize in specific habitats, the latter of which may drive distinct morphology (Best et al., 1990c, 1990b; Howell, 1938). *A. h. harrisii* and *A. l. cinnamomeus* exhibit larger tympanic bullae and longer, narrower nasals than *A. interpres* (Fig. 7)—likely adaptations to greater aridity, enhancing auditory sensitivity in open habitats and respiratory water conservation, as documented in other desert rodents (Alhajeri and Steppan, 2018; Webster and Webster, 1980).

Ammospermophilus species exhibit broad dietary flexibility that potentially influences their craniodental morphology, with diets varying seasonally and by species to include seeds, fruits, vegetation, insects, and occasional small vertebrates (Belk and Smith, 1991; Best et al., 1990c, 1990d; Bowers et al., 2007; Ceballos, 2014; Howell, 1938; Nowak and Paradiso, 1983). Menéndez *et al.* (2023) classified antelope squirrels as primarily granivorous but with distinct feeding strategies: *A. harrisii*, *A. interpres*, and *A. leucurus* specialize as dry fruit eaters that crush seeds and nuts (the ancestral squirrel diet), while *A. nelsoni* functions as a mixed feeder, consuming both grasses and seeds/nuts through crushing and grinding processes. In rodents, dietary specialization correlates with craniodental morphology: generalists have intermediate skull shapes, while specialists exhibit more divergent forms (Cox et al., 2012; Maestri et al., 2016; McLean et al., 2018; Menéndez et al., 2023). However, my results reveal relatively subtle differences in cranial structure among *Ammospermophilus* feeding strategies, suggesting stronger non-dietary selective pressures on skull evolution. The absence of pronounced differences in bite-force-related features (rostra, incisors, maxilla, zygomatic arches) (Figs. 6, 7) that typically distinguish dietary specialists in rodents (Maestri et al., 2016; Mitchell et al., 2024) likely reflects substantial dietary overlap among antelope squirrels, as in both feeding strategies, seeds are consumed despite their different classifications (Menéndez et al., 2023). Alternatively, cheek pouch evolution may promote an alternative avenue for niche divergence through size-related differences, since larger pouches can accommodate larger seeds (Best et al., 1990c, 1990d; Nowak and Paradiso, 1983).

Habitat structure may exert a stronger selective pressure on *Ammospermophilus* cranial shape than diet, as clustering based on taxon-mean shapes (Fig. 7) correlates better with habitat-associated vocalization patterns than feeding ecology. Species inhabiting open desert environments (*A. leucurus* and *A. harrisii*) display relatively shorter, smaller rostra and narrower zygomatic arches (Fig. 7) compared to species from closed rocky or prairie habitats (*A. nelsoni*, *A. interpres*, and *A. insularis*) which are more variable (Bolles, 1988). These morphological distinctions likely reflect adaptational responses to soil characteristics, as the loose sandy soils of desert habitats require fewer cranial specializations for digging than the harder soils of prairie or rocky habitats, which typically require wider zygomatic arches to attach stronger masticatory muscles for incisor-assisted burrowing (see Gomes Rodrigues and Damette, 2023). Cranial evolution in *Ammospermophilus* thus reflects both niche conservatism and divergence, driven by various ecological factors that interact with phylogenetic history and geographic distribution in taxon-specific ways.

Geographic isolation

Geographical isolation appears to accelerate cranial divergence in *Ammospermophilus* taxa, with the Espíritu Santo Island-endemic *A. l. insularis* providing evidence for increased morphological evolution. This island taxon exhibits pronounced cranial and dental divergence from mainland relatives, characterized by larger skull size, a broad rostrum, heavy frontal area, and rudimentary or absent anterior premolars (Álvarez-Castañeda, 2007; Best et al., 1990a; Howell, 1938). Such distinctive morphological traits developed under relatively recent insular isolation (~6,900 years ago) and align with predictions of the Island Syndrome, where isolated populations undergo accelerated morphological change (Adler and Levins, 1994). This morphological distinctiveness corresponds with genetic divergence data that supports elevating *A. l. insularis* to species status (Mantooth et al., 2013).

Unlike mainland *A. harrisii* subspecies that showed no significant cranial differences among them, *A. l. insularis* diverges significantly from its mainland counterpart *A. l. leucurus* in both cranial size (dorsal view) and shape (both views) (Table S2). This island taxon exhibits extreme cranial shape differentiation, occupying a distinctive position along ventral PC1, characterized by longer nasals, shorter incisive bones, smaller molar rows, less flared zygomatic arches, deflated tympanic bullae, smaller foramina magna, and expanded rostra versus reduced braincases (Fig. 6b). The magnitude of this morphological divergence is evidenced by the 100% classification accuracy in both dorsal and ventral analyses, in contrast to the frequent misclassifications observed among mainland subspecies (Table S3). In the composite dendrogram combining dorsal and ventral mean-shape data, *A. l. insularis* diverges first, distinguished by a broad rostrum, enlarged palatine fissures, uniquely shaped zygomatic arches, and the smallest tympanic bullae (Fig. 7), further supporting its cranial distinction.

Beyond its geographical isolation, *A. l. insularis* occupies a unique ecological niche, characterized by distinctive climatic conditions—warmer, wetter environments with high rainfall seasonality, but low temperature variation (Fig. 8). This ecological distinctiveness, combined with insular isolation, likely accelerates cranial evolution, supporting my third hypothesis that geographic isolation promotes cranial divergence in *Ammospermophilus* through the dual mechanisms of genetic drift and local adaptation. *A. l. insularis* represents an incipient species, displaying classic island-driven adaptations (Adler and Levins, 1994; Álvarez-Castañeda, 2007), with the multiple lines of evidence discussed above (extreme cranial divergence in both size and shape, genetic distinctiveness, and ecological specialization) all supporting this conclusion. Given this comprehensive evidence for differentiation across multiple biological dimensions, *A. l. insularis* merits formal recognition and conservation as a distinct species.

Peripheral isolation has similarly driven pronounced cranial divergence in *A. nelsoni*, despite this species sharing a genetic lineage with *A. leucurus* (Figs. 1, 2). This San Joaquin Valley-endemic exhibits distinctive cranial shape features that cause it to split early from other taxa in the combined dorsal–ventral dendrogram, including broader crania and zygomatic arches, proportionally the largest tympanic bullae, and longer nasal bones—all contrasting with the less distinctive shapes of non-isolated lineages (Fig. 7). This cranial shape differentiation, combined with larger cranial size, and unique vocal traits, likely resulted from prolonged geographical isolation dating back to the early Pliocene (Best et al., 1990d; Bolles, 1988; Howell, 1938; Mantooth et al., 2013). Notably, insular *A. l. insularis* and peripheral *A. nelsoni* both possess the largest crania among all sampled taxa (Fig. 4), aligning with predictions from the “Island Rule” where geographic isolation promotes morphological divergence regardless of isolation mechanism (Adler and Levins, 1994; Álvarez-Castañeda, 2007). These findings support the view that peripheral isolation accelerates cranial divergence in *A. nelsoni*, likely driven by local adaptation to the San Joaquin Valley’s distinctive environment. Parallel divergence patterns in insular and peripheral taxa highlight geographic isolation’s central role in generating ecomorphological diversity in *Ammospermophilus*.

Both geographically isolated *Ammospermophilus* taxa face significant conservation challenges, with *A. l. insularis* officially listed as threatened and *A. nelsoni* classified as endangered (Álvarez-Castañeda, 2007; Best et al., 1990a, 1990d; Ceballos, 2014; Hafner et al., 1998; Mantooth et al., 2013). *A. nelsoni* has lost >80% of its historical San Joaquin Valley range and now persists only in small, fragmented populations confined to remnant and marginal habitats (Best et al., 1990d; Hafner et al., 1998). Similarly, *A. l. insularis* faces exceptional vulnerability due to its strict confinement to Espíritu Santo Island, where any habitat disturbance could have severe consequences for this recently diverged taxon (Álvarez-Castañeda, 2007; Best et al., 1990a; Ceballos, 2014; Mantooth et al., 2013). Conservation priority for both taxa is justified by their pronounced genetic, morphological, and behavioral distinctiveness, coupled with their narrow, isolated distributions—characteristics that make them unique components of sciurid phylogenetic diversity (Bolles, 1988; Howell, 1938; Mantooth et al., 2013).

Conclusion

This study shows that *Ammospermophilus*’ cranial variation reflects multiple interacting evolutionary forces. Allometric scaling drives species differentiation in patterns similar to those observed in other rodent taxa. Ventral cranial shape is more phylogenetically conserved and provides greater taxonomic resolution than dorsal shape, potentially reflecting distinct functional constraints in different cranial regions. Environmental factors significantly influence morphological variation, with *A. leucurus* showing particularly strong climate-shape relationships, likely reflecting its broad geographic distribution. The enlarged tympanic bullae observed in taxa inhabiting drier environments likely reflect functional adaptations. Geographic isolation appears to accelerate morphological divergence, as evidenced by the distinctive cranial characteristics of both insular *A. l. insularis* and peripheral *A. nelsoni*, highlighting their conservation significance. These results advance our understanding of cranial evolution by revealing how morphological diversification emerges from complex interactions between phylogenetic history, allometric scaling, ecological adaptation, and geographic isolation, with cranial regions responding differentially to these evolutionary pressures.

Data availability

Data produced in this study have been deposited in the supplementary materials (Data S1).

Conflict of interest

The author declares no conflict of interest.

Acknowledgments

I thank staff at AMNH, FMNH, MVZ, UF, and USNM for assistance during museum visits. Kuwait University provided scientific leave (2019-2020) and supported travel to the USNM. Kuwait University also approved a 2024-2025 sabbatical, which was crucial for completing this work. I also acknowledge the comments of two anonymous reviewers. This research received no grant funding.

References

Adams, D., Collyer, M., Kaliontzopoulou, A., Baken, E., 2024. geomorph: geometric morphometric analyses of 2D and 3D landmark data [WWW Document]. URL https://cran.r-project.org/web/packages/geomorph/index.html

Adler, G.H., Levins, R., 1994. The Island Syndrome in Rodent Populations. Q Rev Biol 69, 473–490.

Alhajeri, B.H., 2025a. Interspecific cranial variation in coarse-haired pocket mice (*Chaetodipus*): a geometric morphometric analysis within a phylogenetic framework. Mamm Biol 105, 449–466. https://doi.org/10.1007/s42991-025-00490-2

Alhajeri, B.H., 2025b. Cranial variation in species and subspecies of kangaroo rats (*Dipodomys*, Dipodomyinae, Rodentia) according to geometric morphometrics. Integr Zool 20, 108–134. https://doi.org/10.1111/1749-4877.12824

Alhajeri, B.H., 2023. Cranial geometric morphometrics of jumping mice (Genera: *Eozapus*, *Napaeozapus*, and *Zapus*; Zapodinae, Rodentia): Implications for subspecies conservation. J Mamm Evol 30, 713–734. https://doi.org/10.1007/s10914-023-09666-4

Alhajeri, B.H., 2022. Geometric differences between the crania of Australian hopping mice (*Notomys*, Murinae, Rodentia). Aust Mammal 44, 24–38. https://doi.org/10.1071/AM20067

Alhajeri, B.H., 2021a. A geometric morphometric analysis of geographic mandibular variation in the dwarf gerbil *Gerbillus nanus* (Gerbillinae, Rodentia). J Mamm Evol 28, 469–480. https://doi.org/10.1007/s10914-020-09530-9

Alhajeri, B.H., 2021b. Cranial variation in allactagine jerboas (Allactaginae, Dipodidae, Rodentia): a geometric morphometric study. Zool Res 42, 182–194. https://doi.org/10.24272/j.issn.2095-8137.2020.302

Alhajeri, B.H., 2021c. A morphometric comparison of the cranial shapes of Asian dwarf hamsters (*Phodopus*, Cricetinae, Rodentia). Zool Anz 292, 184–196. https://doi.org/10.1016/j.jcz.2021.04.001

Alhajeri, B.H., 2019. Cranial variation in geographically widespread dwarf gerbil *Gerbillus nanus* (Gerbillinae, Rodentia) populations: Isolation by distance versus adaptation to local environments. J Zool Syst Evol Res 57, 191–203. https://doi.org/10.1111/jzs.12247/

Alhajeri, B.H., Alaqeely, R., Alhaddad, H., 2025. Geometric morphometrics of silky pocket mice (*Perognathus*: Perognathinae: Rodentia) crania reveals new insights into their variation, evolution, and taxonomy. Zool J Linn Soc 203, zlae029. https://doi.org/10.1093/zoolinnean/zlae029

Alhajeri, B.H., Hasan, Z., Alhaddad, H., 2023. Cranial differences in three-toed jerboas (Dipodinae, Dipodidae, Rodentia) according to recent taxonomic revisions. Curr Zool 69, 475–490. https://doi.org/10.1093/cz/zoac057

Alhajeri, B.H., Hunt, O.J., Steppan, S.J., 2015. Molecular systematics of gerbils and deomyines (Rodentia: Gerbillinae, Deomyinae) and a test of desert adaptation in the tympanic bulla. J Zool Syst Evol Res 53, 312–330. https://doi.org/10.1111/jzs.12102/

Alhajeri, B.H., Steppan, S.J., 2025. Cranial variation across spiny pocket mice (*Heteromys*, *Liomys*) in new phylogenetic and taxonomic perspectives. Zoology 168, 126238. https://doi.org/10.1016/j.zool.2025.126238

Alhajeri, B.H., Steppan, S.J., 2018. A phylogenetic test of adaptation to deserts and aridity in skull and dental morphology across rodents. J Mammal 99, 1197–1216. https://doi.org/10.1093/jmammal/gyy099

Alhajeri, B.H., Steppan, S.J., 2016. Association between climate and body size in rodents: A phylogenetic test of Bergmann’s rule. Mamm Biol 81, 219–225. https://doi.org/10.1016/j.mambio.2015.12.001

Álvarez-Castañeda, S.T., 2007. Systematics of the antelope ground squirrel (*Ammospermophilus*) from islands adjacent to the Baja California peninsula. J Mammal 88, 1160–1169. https://doi.org/10.1644/06-MAMM-A-065R3.1

Belk, M.C., Smith, H.D., 1991. *Ammospermophilus leucurus*. Mamm Species 1–8. https://doi.org/10.2307/3504191

Bertrand, O.C., Püschel, H.P., Schwab, J.A., Silcox, M.T., Brusatte, S.L., 2021. The impact of locomotion on the brain evolution of squirrels and close relatives. Commun Biol 4. https://doi.org/10.1038/s42003-021-01887-8

Best, T.L., Caesar, K., Titus, A.S., Lewis, C.L., 1990a. *Ammospermophilus insularis*. Mamm Species 1–4. https://doi.org/10.1093/mspecies/364.1

Best, T.L., Lewis, C.L., Caesar, K., Titus, A.S., 1990b. *Ammospermophilus interpres*. Mamm Species 1–6. https://doi.org/10.1093/mspecies/365.1

Best, T.L., Titus, A.S., Caesar, K., Lewis, C.L., 1990c. *Ammospermophilus harrisii*. Mamm Species 1–7. https://doi.org/10.2307/3504155

Best, T.L., Titus, A.S., Lewis, C.L., Caesar, K., 1990d. *Ammospermophilus nelsoni*. Mamm Species 1–7. https://doi.org/10.2307/3504314

Blomberg, S.P., Garland, T.J., Ives, A.R., 2003. Testing for phylogenetic signal in comparative data: behavioral traits are more labile. Evolution (N Y) 57, 717–745.

Bolles, K., 1988. Evolution and variation of antipredator vocalisations of Antelope squirrels, *Ammospermophilus* (Rodentia: Sciuridae). Zeitschrift für Säugetierkd 53, 129–147.

Bowers, N., Bowers, R., Kaufman, K., 2007. Kaufman Field Guide to Mammals of North

America. Houghton Mifflin, Boston, Massachusetts.

Cardini, A., 2019. Craniofacial allometry is a rule in evolutionary radiations of placentals. Evol Biol 46, 239–248. https://doi.org/10.1007/s11692-019-09477-7

Cardini, A., O'Higgins, P., 2004. Patterns of morphological evolution in Marmota (Rodentia, Sciuridae): geometric morphometrics of the cranium in the context of marmot phylogeny, ecology and conservation. Biol J Linn Soc 82, 385–407.

Ceballos, G., 2014. Mammals of Mexico. Johns Hopkins University Press, Baltimore.

Collyer, M.L., Adams, D.C., 2018. RRPP: an R package for fitting linear models to high-dimensional data using residual randomization. Methods Ecol Evol 9, 1772–1779. https://doi.org/doi:10.1111/2041-210X.13029/

Cox, P.G., Rayfield, E.J., Fagan, M.J., Herrel, A., Pataky, T.C., Jeffery, N., 2012. Functional evolution of the feeding system in rodents. PLoS One 7. https://doi.org/10.1371/journal.pone.0036299

Dashti, Z., Alhaddad, H., Alhajeri, B.H., 2022a. Skull variation in populations of the Indian gerbil *Tatera indica* (Gerbillinae, Rodentia) sampled across its broad geographic range. Vertebr Zool 72, 1077–1098. https://doi.org/10.3897/vz.72.e90474

Dashti, Z., Alhaddad, H., Alhajeri, B.H., 2022b. A geometric morphometric analysis of geographic variation in the Cape short-eared gerbil, *Desmodillus auricularis* (Rodentia: Gerbillinae). Mammalia, Mammalia 86, 615–631. https://doi.org/doi:10.1515/mammalia-2022-0019

Drake, A.G., Klingenberg, C.P., 2008. The pace of morphological change: historical transformation of skull shape in St Bernard dogs. Proc R Soc B Biol Sci 275, 71–76. https://doi.org/10.1098/rspb.2007.1169

Fick, S.E., Hijmans, R.J., 2017. WorldClim 2: new 1-km spatial resolution climate surfaces for global land areas. Int J Climatol 37, 4302–4315. https://doi.org/10.1002/joc.5086/

Fourcade, Y., Alhajeri, B.H., 2023. Environmental correlates of body size influence range size and extinction risk: A global study in rodents. Glob Ecol Biogeogr 32, 206–217. https://doi.org/https://doi.org/10.1111/geb.13622

Gomes Rodrigues, H., Damette, M., 2023. Incipient morphological specializations associated with fossorial life in the skull of ground squirrels (Sciuridae, Rodentia). J Morphol 284. https://doi.org/10.1002/jmor.21540

Google, 2025. Google Maps. Version 3.59.8 [WWW Document]. URL https://maps.google.com/ (accessed 2.16.25).

Hafner, D.J., Yensen, E., Kirkland, G.L., 1998. North American rodents: status survey and conservation action plan, SSC Status Survey and Conservation Action Plans. International Union for the Conservation of Nature and Natural Resources, Gland, Switzerland.

Hijmans, R.J., 2019. raster: geographic data analysis and modeling [WWW Document]. URL http://cran.r-project.org/package=raster

Howell, A.H., 1938. Revision of the North American ground squirrels: With a classification of the North American Sciuridae (North American fauna), First. ed. USDA Bureau of Biological Survey, Washington, D. C.

Kamilar, J.M., Cooper, N., 2013. Phylogenetic signal in primate behaviour, ecology and life history. Philos Trans R Soc B Biol Sci 368. https://doi.org/10.1098/rstb.2012.0341

Langsrud, Ø., 2003. ANOVA for unbalanced data: use type II instead of type III sums of squares. Stat Comput 13, 163–167. https://doi.org/10.1023/A:1023260610025

Lu, X., Ge, D., Xia, L., Huang, C., Yang, Q., 2014. Geometric morphometric study of the skull shape diversification in Sciuridae (Mammalia, Rodentia). Integr Zool 9, 231–245. https://doi.org/10.1111/1749-4877.12035

Maestri, R., Patterson, B.D., Fornel, R., Monteiro, L.R., de Freitas, T.R.O., 2016. Diet, bite force and skull morphology in the generalist rodent morphotype. J Evol Biol 29, 2191–2204. https://doi.org/10.1111/jeb.12937

Mammal Diversity Database, 2025. Mammal Diversity Database (Version 2.0). Zenodo. https://doi.org/10.5281/zenodo.15007505 [WWW Document]. https://doi.org/10.5281/zenodo.15007505

Mantooth, S.J., Hafner, D.J., Bryson, R.W., Riddle, B.R., 2013. Phylogeographic diversification of antelope squirrels (*Ammospermophilus*) across North American deserts. Biol J Linn Soc 109, 949–967. https://doi.org/10.1111/bij.12084

Marcy, A.E., Guillerme, T., Sherratt, E., Rowe, K.C., Phillips, M.J., Weisbecker, V., 2020. Australian rodents reveal conserved cranial evolutionary allometry across 10 million years of murid evolution. Am Nat 196, 755–768. https://doi.org/10.1101/2020.04.30.071308

Marroig, G., Cheverud, J.M., 2005. Size as a line of least evolutionary resistance: Diet and adaptive morphological radiation in new world monkeys. Evolution (N Y) 59, 1128–1142.

McLean, B.S., Helgen, K.M., Goodwin, H.T., Cook, J.A., 2018. Trait-specific processes of convergence and conservatism shape ecomorphological evolution in ground-dwelling squirrels. Evolution (N Y) 72, 473–489. https://doi.org/10.1111/evo.13422

Menéndez, I., Zelditch, M.L., Tejero-Cicuéndez, H., Swiderski, D.L., Carro-Rodríguez, P.M., Hernández Fernández, M., Álvarez-Sierra, M.Á., Gómez Cano, A.R., 2023. Dietary adaptations and tooth morphology in squirrels: Insights from extant and extinct species. Palaeogeogr Palaeoclimatol Palaeoecol 629. https://doi.org/10.1016/j.palaeo.2023.111788

Mitchell, D.R., Sherratt, E., Weisbecker, V., 2024. Facing the facts: adaptive trade-offs along body size ranges determine mammalian craniofacial scaling. Biol Rev 99, 496–524. https://doi.org/10.1111/brv.13032

Nowak, R.M., Paradiso, J.L., 1983. Walker's mammals of the world. Volume II. Fourth edition, Walker's Mammals of the World. The Johns Hopkins University Press, Baltimore.

Paradis, E., Schliep, K., 2019. ape 5.0: an environment for modern phylogenetics and evolutionary analyses in R. Bioinformatics 35, 526–528. https://doi.org/10.1093/bioinformatics/bty633/

R Core Team, 2024. R: a language and environment for statistical computing. R Foundation for Statistical Computing, Vienna, Austria [WWW Document]. URL https://www.r-project.org/

Rensch, B., 1948. Histological Changes Correlated with Evolutionary Changes of Body Size. Evolution (N Y) 2, 218–230. https://doi.org/https://doi.org/10.1111/j.1558-5646.1948.tb02742.x

Rohlf, F.J., 2015. The tps series of software. Hystrix 26, 1–4. https://doi.org/10.4404/hystrix-26.1-11264

Rohlf, F.J., Corti, M., 2000. Use of two-block partial least-squares to study covariation in shape. Syst Biol 49, 740–753. https://doi.org/10.1080/106351500750049806

Rohlf, F.J., Slice, D., 1990. Extensions of the procrustes method for the optimal superimposition of landmarks. Syst Biol 39, 40–59. https://doi.org/10.2307/2992207/

Schneider, C.A., Rasband, W.S., Eliceiri, K.W., 2012. NIH Image to ImageJ: 25 years of image analysis. Nat Methods 9, 671–675. https://doi.org/10.1038/nmeth.2089/

Sinitsa, M. V., Pogodina, N. V., Kryuchkova, L.Y., 2019. The skull of *Spermophilus nogaici* (Rodentia: Sciuridae: Xerinae) and the affinities of the earliest Old World ground squirrels.

Zool J Linn Soc 186, 826–864. https://doi.org/10.1093/zoolinnean/zly092

Sneath, P.H.A., Sokal, R.R., 1973. Numerical taxonomy. Freeman, San Francisco.

South, A., 2017. rnaturalearth: world map data from natural earth [WWW Document]. URL https://cran.r-project.org/package=rnaturalearth

Tavares, W.C., Pessôa, L.M., Seuánez, H.N., 2019. Changes in Ontogenetic Allometry and their Role in the Emergence of Cranial Morphology in Fossorial Spiny Rats (Echimyidae, Hystricomorpha, Rodentia). J Mamm Evol 26, 575–585. https://doi.org/10.1007/s10914-018-9433-1

Venables, W.N., Ripley, B.D., 2002. Modern applied statistics with S. Fourth edition. Springer, New York.

Webster, D.B., Webster, M., 1980. Morphological adaptations of the ear in the rodent family heteromyidae. Integr Comp Biol 20, 247–254. https://doi.org/10.1093/icb/20.1.247

Wickham, H., 2016. ggplot2: elegant graphics for data analysis. Springer-Verlag New York, New York.

Wilson, D.E., Reeder, D.M., 2005. Mammal Species of the World. A Taxonomic and Geographic Reference, Third. ed. Johns Hopkins University Press.

Wilson, L.A.B., 2013. Allometric disparity in rodent evolution. Ecol Evol 3, 971–984. https://doi.org/10.1002/ece3.521

Wright, S., 1943. Isolation by Distance. Genetics 28, 114–138.

Zelditch, M.L., Swiderski, D.L., Sheets, H.D., 2012. Geometric morphometrics for biologists: a primer. Second edition. Academic Press, Massachusetts.

Tables

Table 1. ANOVA results for four linear models: (a) centroid size by species (both views) and (b) Procrustes coordinates with centroid size, species, and their interaction as predictors (both views).

Table 2. Pairwise species mean distances with statistics for (a) centroid size, (b) Procrustes coordinates, and (c) Procrustes coordinates adjusted for common and unique allometries.

Figures

Fig. 1. *Ammospermophilus* relationships based on molecular phylogenies from (a) Mantooth *et al.* (2013; six species) and (b) McLean *et al.* (2018; five species). Relationships are shown as simplified cladograms with arbitrary branch lengths. The Mantooth *et al.* cladogram derives from multi-locus analyses (their Figs. 4 and 5), with species not sampled in the present study shown in gray. The McLean *et al.* cladogram is based on their Fig. 1. Cladograms were generated using the R library ape (Paradis and Schliep, 2019).

Fig. 2. Locality map of sampled specimens with species shown by symbols and subspecies by colors. Geographic coordinates are in Data S1. See Fig. S1 for a zoomed-out map. Map generated using ggplot2 and rnaturalearth.

Fig. 3. Cranium of Texas antelope squirrel *Ammospermophilus interpres* (USNM 119910) from San Andres Mountains, New Mexico, showing landmark positions on (a) dorsal and (b) ventral views. Landmark descriptions appear in Table S1.

Fig. 4. Boxplots of centroid sizes for (a) dorsal and (b) ventral cranial views by taxon. Boxes show medians and quartiles, whiskers extend to values ≤ 1.5 × inter-quartile range, and points represent outliers. Boxes are colored corresponding to the color of the most sampled subspecies within each species (matching Fig. 2). Plot created in ggplot2.

Fig. 5. Shape-size covariation scatterplots for (a) dorsal and (b) ventral views. Standardized shape scores (RegScore; Drake and Klingenberg, 2008) are plotted against centroid size. Species are indicated by symbols and subspecies by colors (matching Fig. 2). TPS deformations at axis extremes display shape variation (5× magnified) with connected landmarks to improve interpretability. The species-unique allometry model (shape ~ size × species; Table 1b) allows

different allometric trajectories per species rather than forcing a common slope. Species-specific regression lines are color-coded by the predominant subspecies. Plot generated using geomorph.

Fig. 6. PC1–2 scatterplots of (a) dorsal and (b) ventral Procrustes coordinates. Species are indicated by symbols and subspecies by colors (matching Fig. 2). Variance explained by PC1–2 is indicated. TPS deformations at axis extremes display shape variation (3× magnified) with connected landmarks to improve interpretability. The mean landmark configuration based on all specimens is shown for each view. Plots generated in geomorph.

Fig. 7. UPGMA dendrogram based on the average of dorsal and ventral taxon-mean Procrustes distance matrices. The TPS deformations at tip labels are of taxon-mean shapes compared to the average of all seven taxon-mean shapes (3× magnified with connected landmarks). Tips are color-coded by predominant subspecies (matching Fig. 2). Dorsal views are shown in blue, while ventral views are depicted in green. Plot generated using geomorph and base R libraries.

Fig. 8. PC1–2 scatterplots of climate data with species shown by symbols and subspecies by colors (matching Fig. 2). Variance explained by PC1–2 is shown. Overlapping points (specimens from the same localities with identical climate data) are represented by larger symbols (using a consistent scaling factor). PCA is based on 19 standardized bioclimatic variables (centered, scaled) from WorldClim (version 2; Fick and Hijmans, 2017) described in Table S4 (which also list the PCA loadings). The plot summarizes the main climatic patterns at axis extremes (based on PCA loadings). Plot generated using geomorph.

Appendix and supporting information

The appendix, supporting tables, figures, and data are provided separately.

Table 1. ANOVA results for four linear models: (a) centroid size by species (both views) and (b) Procrustes coordinates with centroid size, species, and their interaction as predictors (both views).

	df	SS	MS	R^2	F	Z	p
a. Centroid size (log)							
[Dorsal view]							
Species	3	0.035094	0.011698	0.12193	6.7119	3.1701	0.001
Residuals	145	0.252718	0.001743	0.87807			
Total	148	0.287812					
[Ventral view]							
Species	3	0.08258	0.027528	0.2134	13.022	4.8786	0.001
Residuals	144	0.3044	0.002114	0.7866			
Total	147	0.38698					
b. Procrustes shape							
[Dorsal view]							
Size	1	0.002981	0.002981	0.01846	3.1597	3.2002	0.004
Species	3	0.019179	0.006393	0.11875	6.7754	7.1014	0.001
Size × species	3	0.0051	0.0017	0.03158	1.8019	2.5834	0.006
Residuals	141	0.133039	0.000944	0.82374			
Total	148	0.161506					
[Ventral view]							
Size	1	0.003223	0.003223	0.02127	4.016	4.0144	0.001
Species	3	0.031101	0.010367	0.20523	12.9171	9.7821	0.001
Size × species	3	0.003229	0.001076	0.02131	1.3412	1.529	**0.057**
Residuals	140	0.112361	0.000803	0.74146			
Total	147	0.151539					

Notes: df=degrees of freedom; SS=sequential sums of squares for centroid size models and hierarchical sums of squares for Procrustes coordinates models; MS=mean squares; R^2=R-squared values; F=F-values; Z=effect sizes (standard deviates of F sampling distributions); p=p-values based on 999 permutations. RRPP was used to evaluate the fit of each linear model. Ordinary least squares (OLS) were used to estimate model coefficients. All model terms are significant ($p<0.05$), except for one, which was marginally significant is highlighted in bold. These models omit specimens damaged in either view (from the respective view).

Table 2. Pairwise species mean distances with statistics for (a) centroid size, (b) Procrustes coordinates, and (c) Procrustes coordinates adjusted for common and unique allometries.

	(a) Size				(b) Shape (no correction)				(c) Shape (correction)			
	d	UCL	Z	p	d	UCL	Z	p	d	UCL	Z	p
I. Dorsal view												
A. harrisii — *A. interpres*	0.006	0.021	-0.082	0.552	0.014	0.011	2.897	**0.003**	0.014	0.018	-1.073	0.858
A. harrisii — *A. leucurus*	0.001	0.020	-1.280	0.885	0.017	0.010	4.448	**0.001**	0.017	0.022	-0.693	0.743
A. harrisii — *A. nelsoni*	0.036	0.021	2.675	**0.001**	0.023	0.010	5.723	**0.001**	0.020	0.027	-1.749	0.960
A. interpres — *A. leucurus*	0.008	0.020	0.160	0.450	0.021	0.010	5.434	**0.001**	0.021	0.025	-0.555	0.697
A. interpres — *A. nelsoni*	0.030	0.020	2.261	**0.006**	0.025	0.010	6.104	**0.001**	0.022	0.028	-1.536	0.935
A. leucurus — *A. nelsoni*	0.037	0.020	2.905	**0.001**	0.014	0.010	3.407	**0.002**	0.013	0.019	-1.269	0.896
II. Ventral view												
A. harrisii — *A. interpres*	0.001	0.025	-1.864	0.970	0.026	0.011	5.248	**0.001**	0.026	0.030	-0.411	0.649
A. harrisii — *A. leucurus*	0.003	0.023	-0.945	0.800	0.015	0.010	3.480	**0.001**	0.016	0.019	-0.349	0.625
A. harrisii — *A. nelsoni*	0.054	0.025	3.174	**0.001**	0.024	0.011	4.734	**0.001**	0.027	0.031	-0.132	0.558
A. interpres — *A. leucurus*	0.003	0.023	-0.854	0.784	0.020	0.010	4.431	**0.001**	0.020	0.024	-1.042	0.844
A. interpres — *A. nelsoni*	0.053	0.024	3.264	**0.001**	0.033	0.011	6.153	**0.001**	0.035	0.040	0.053	0.480
A. leucurus — *A. nelsoni*	0.056	0.023	3.648	**0.001**	0.026	0.010	4.646	**0.001**	0.030	0.033	0.218	0.417

Notes: d=distances between (least squares) means; UCL=95% upper confidence limit for test statistic (one-tailed); Z=effect sizes; p=p-values based on 999 permutations. Significantly different pairs ($p<0.05$) are in bold. Specimens damaged in either view were excluded (from that view). Procrustes coordinates corrected for common and unique allometries indicate comparisons between least squares means with logged centroid size as a covariate that is also interacting with the species factor.

Figure 1

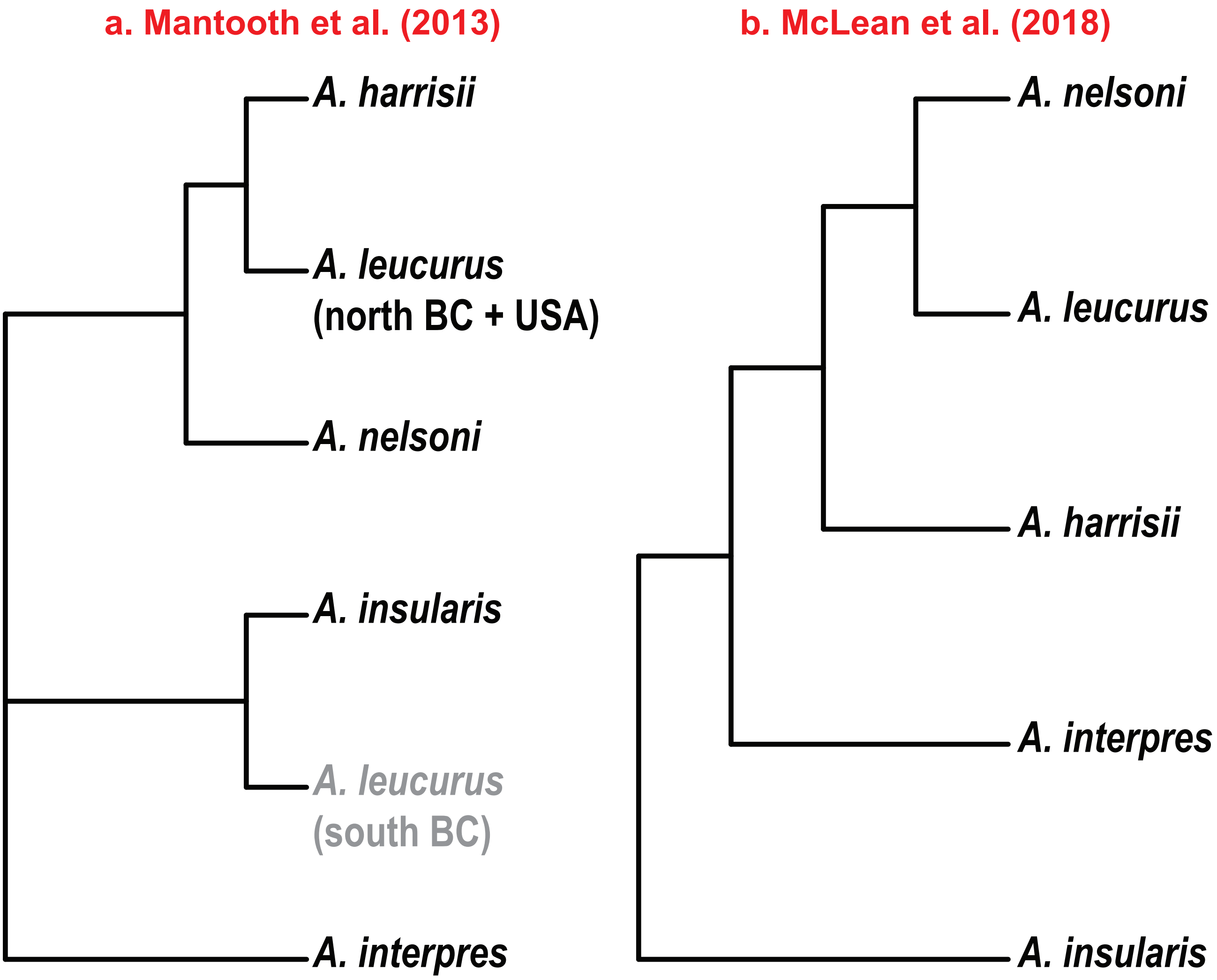
a. Mantooth et al. (2013)
A. harrisii
A. leucurus
(north BC + USA)
A. nelsoni
A. insularis
A. leucurus
(south BC)
A. interpres
b. McLean et al. (2018)
A. nelsoni
A. leucurus
A. harrisii
A. interpres
A. insularis

Figure 2

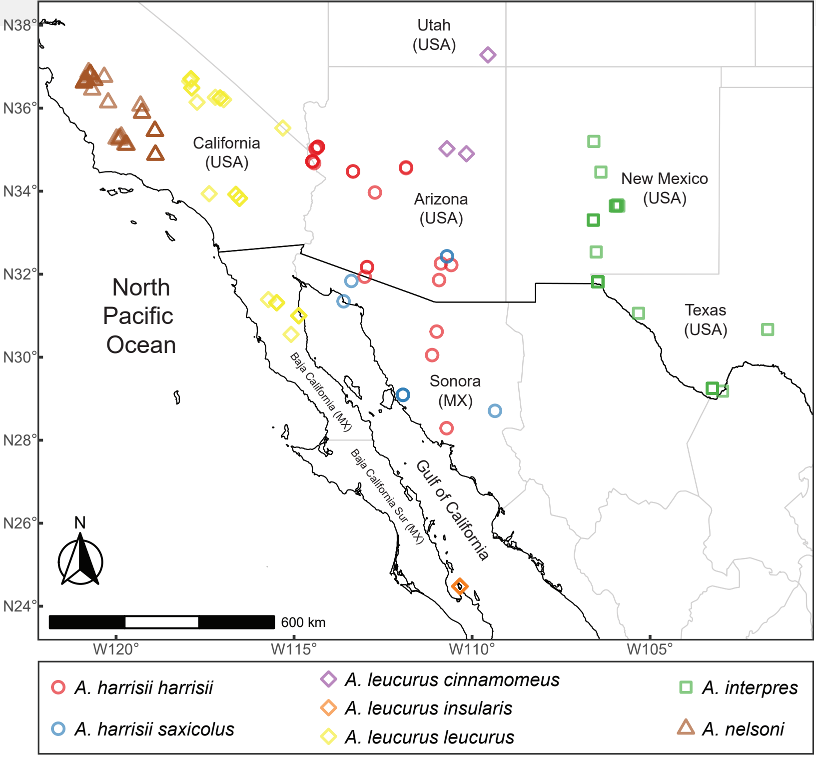
N38°
N36°
N34°
N32°
N30°
N28°
N26°
N24°
W120°
W115°
W110°
W105°
Utah (USA)
California (USA)
Arizona (USA)
New Mexico (USA)
Texas (USA)
Sonora (MX)
Baja California (MX)
Baja California Sur (MX)
Gulf of California
North Pacific Ocean
N
600 km
○ A. harrisii harrisii
○ A. harrisii saxicolus
◇ A. leucurus cinnamomeus
◇ A. leucurus insularis
◇ A. leucurus leucurus
□ A. interpres
△ A. nelsoni

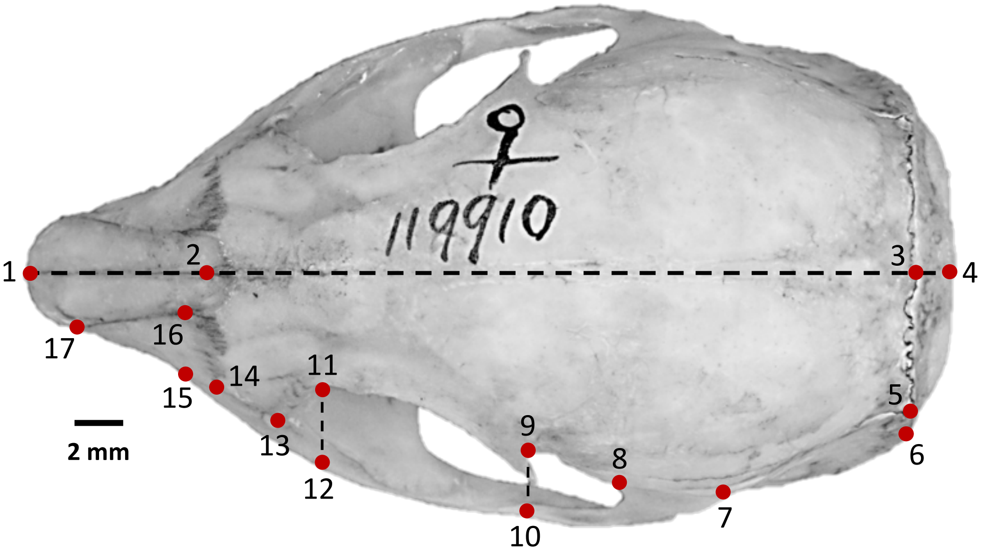
♀
119910
1
2
3
4
5
6
7
8
9
10
11
12
13
14
15
16
17
2 mm

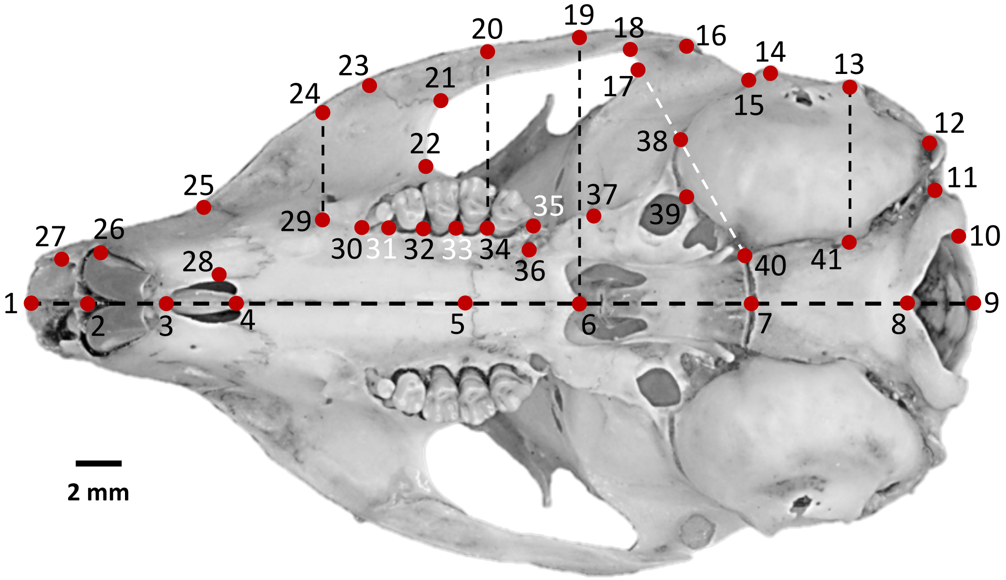
1
2
3
4
5
6
7
8
9
10
11
12
13
14
15
16
17
18
19
20
21
22
23
24
25
26
27
28
29
30
31
32
33
34
35
36
37
38
39
40
41
2 mm

Figure 4

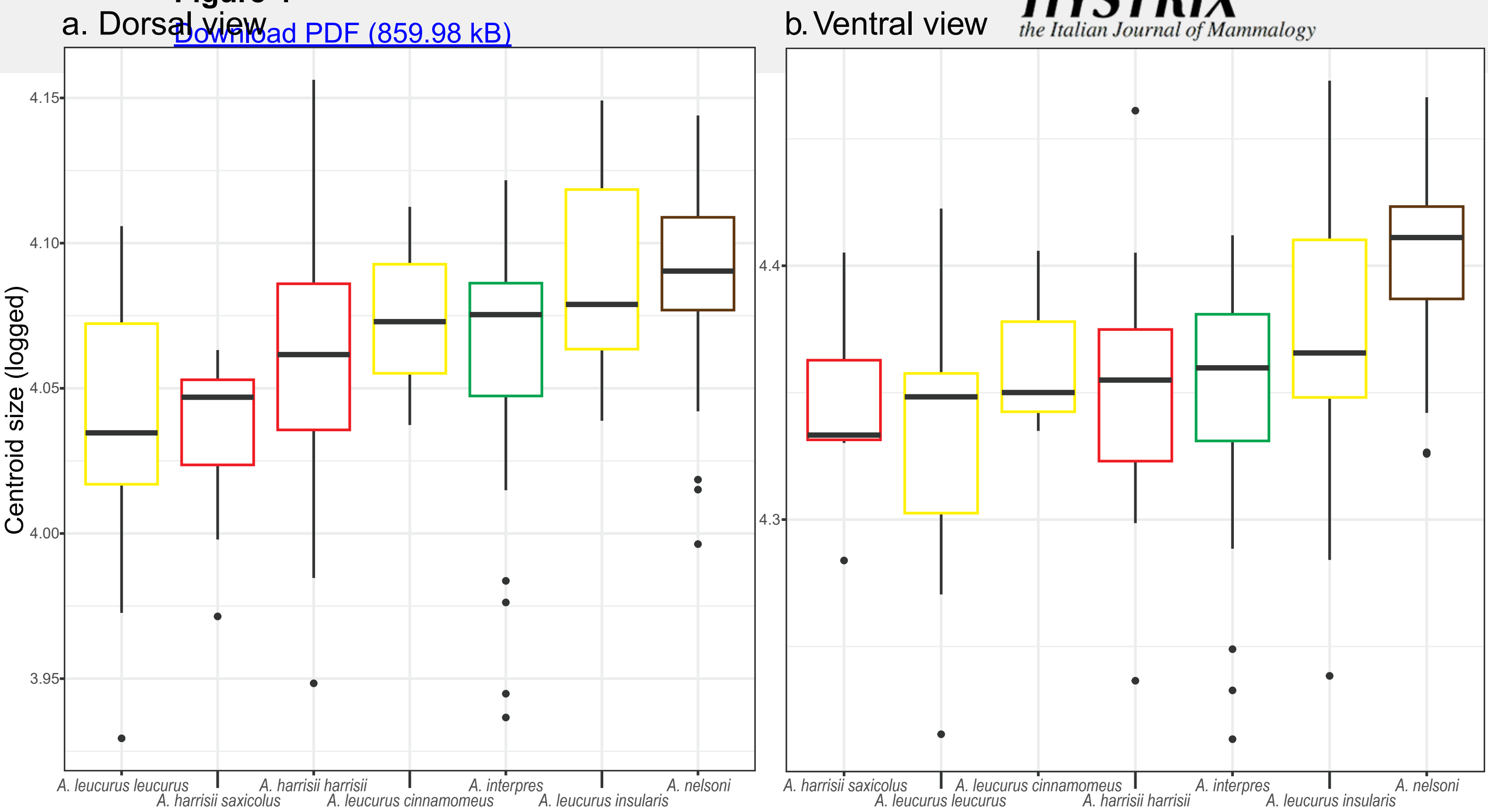
a. Dorsal view
Centroid size (logged)
4.15
4.10
4.05
4.00
3.95
A. leucurus leucurus
A. harrisii saxicolus
A. harrisii harrisii
A. leucurus cinnamomeus
A. interpres
A. leucurus insularis
A. nelsoni
b. Ventral view
4.4
4.3
A. harrisii saxicolus
A. leucurus leucurus
A. leucurus cinnamomeus
A. harrisii harrisii
A. interpres
A. leucurus insularis
A. nelsoni

HYSTRIX
the Italian Journal of Mammalogy

Figure 5

a. Dorsal view

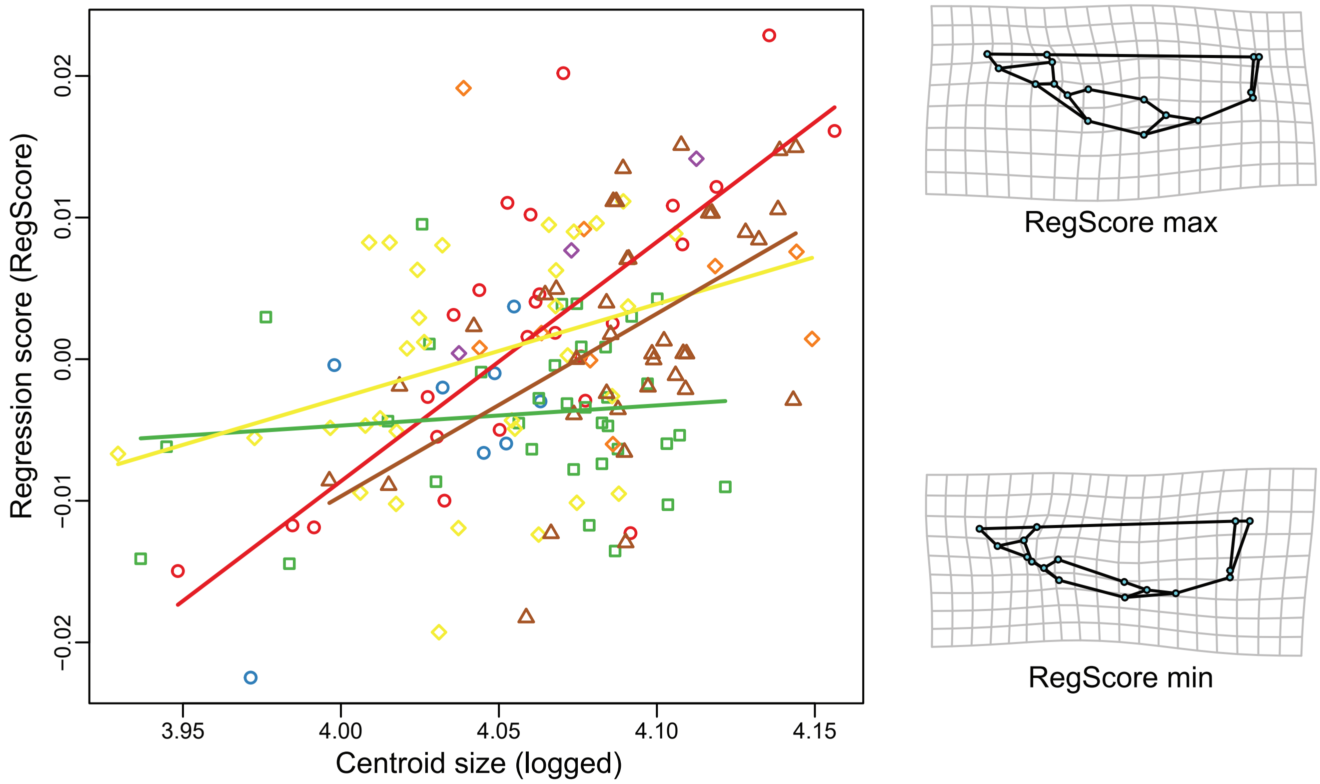

b. Ventral view

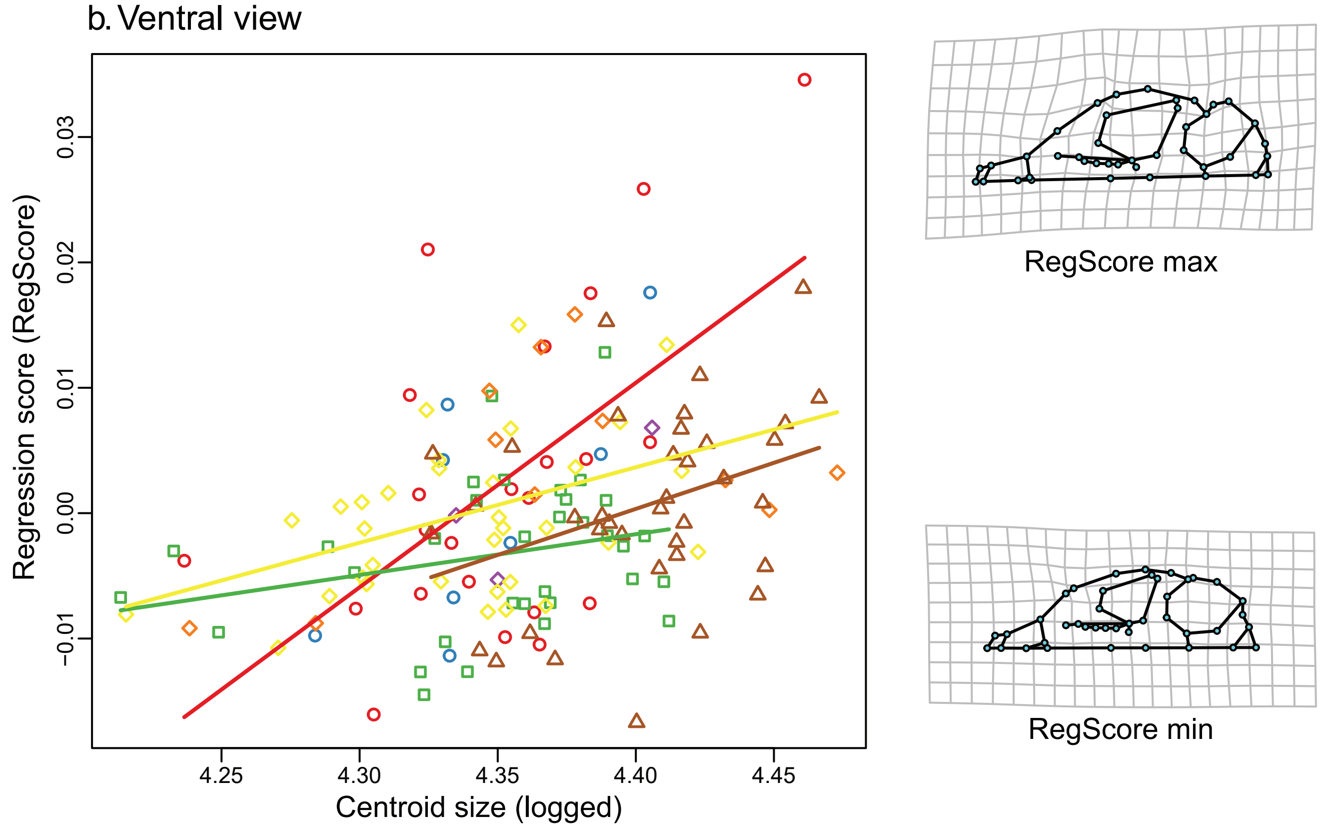

HYSTRIX
the Italian Journal of Mammalogy

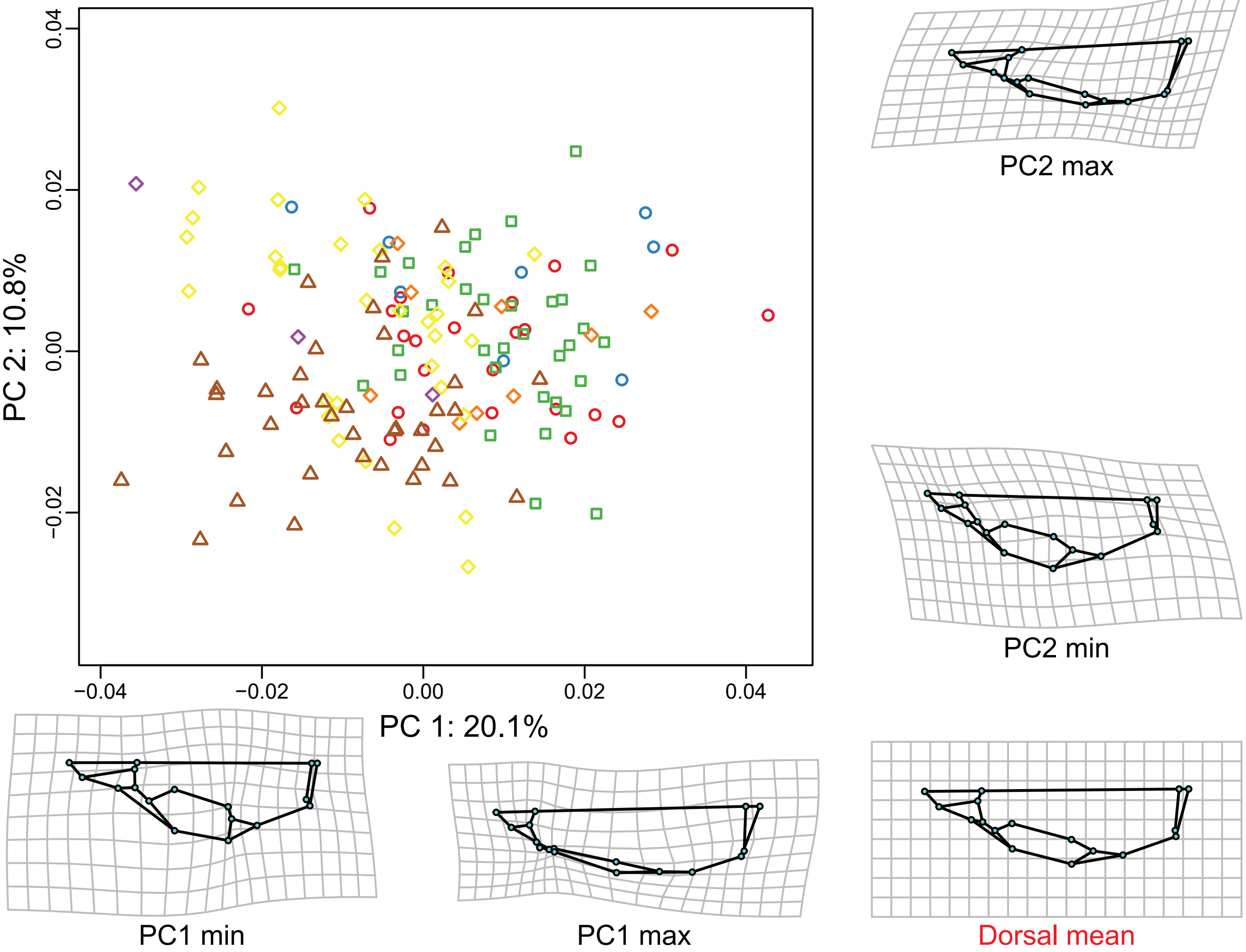
a. Dorsal view

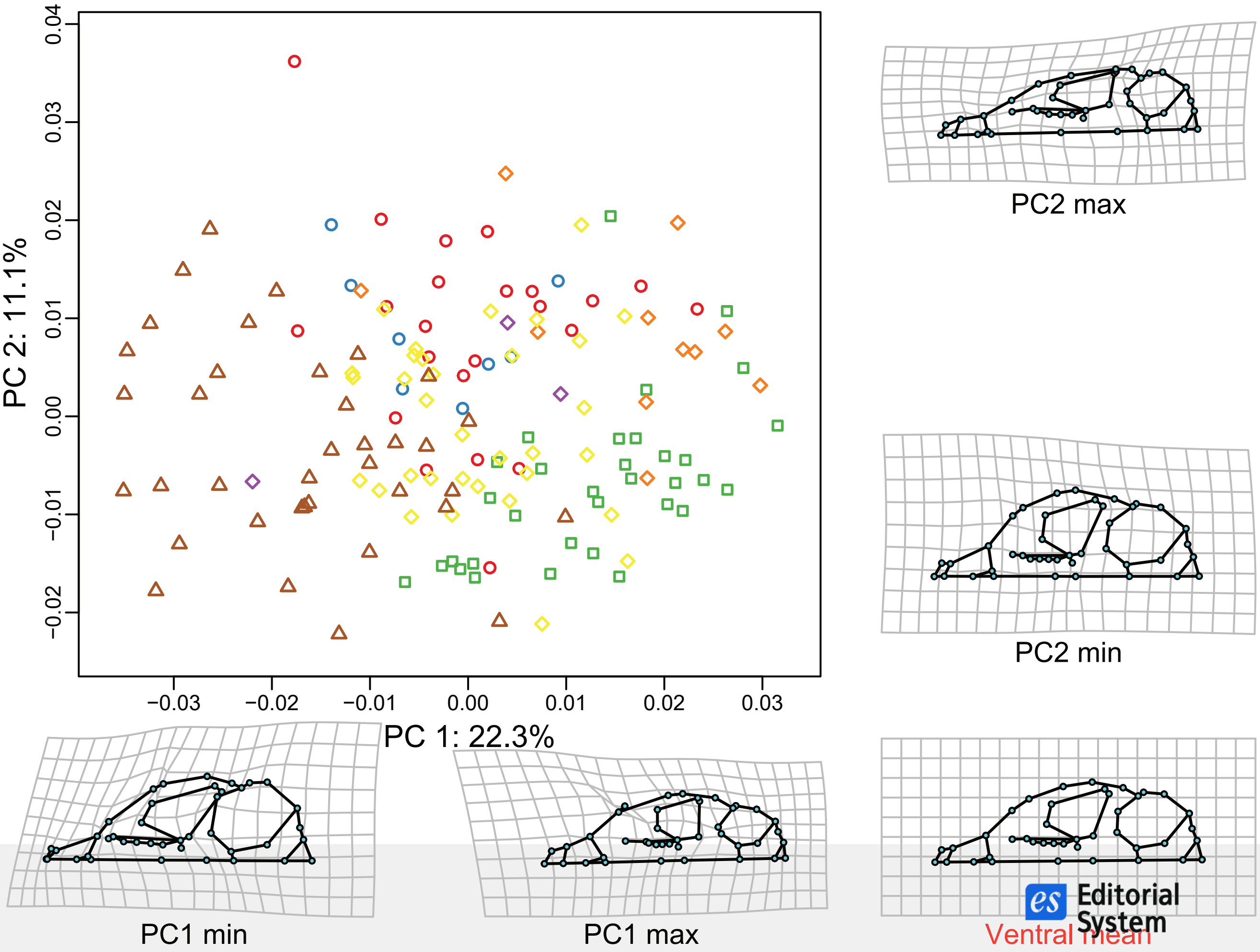
b. Ventral view

Figure 7

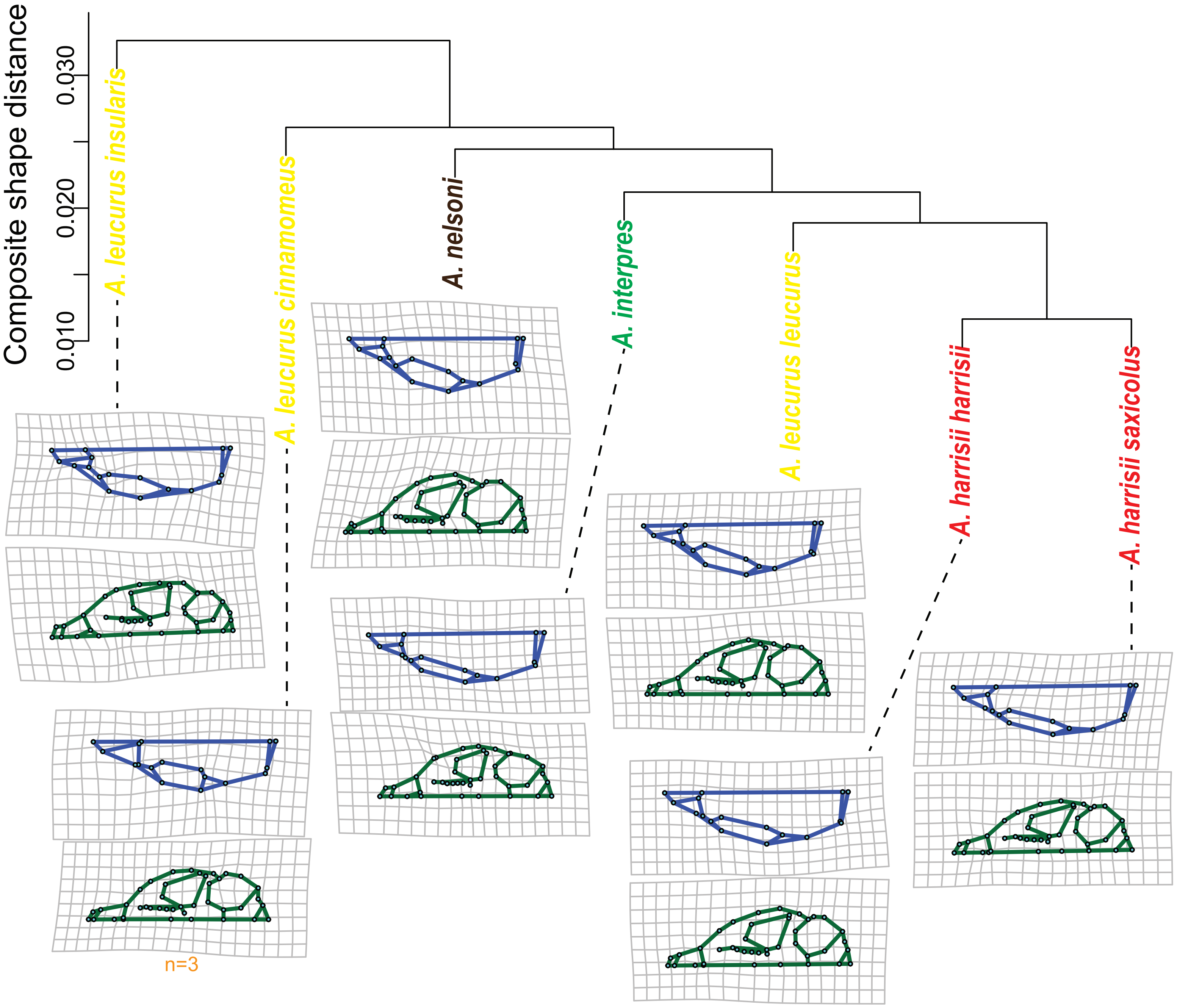
Composite shape distance
0.030
0.020
0.010
A. leucurus insularis
A. leucurus cinnamomeus
A. nelsoni
A. interpres
A. leucurus leucurus
A. harrisii harrisii
A. harrisii saxicolus
n=3

Figure 8

HYSTRIX
the Italian Journal of Mammalogy

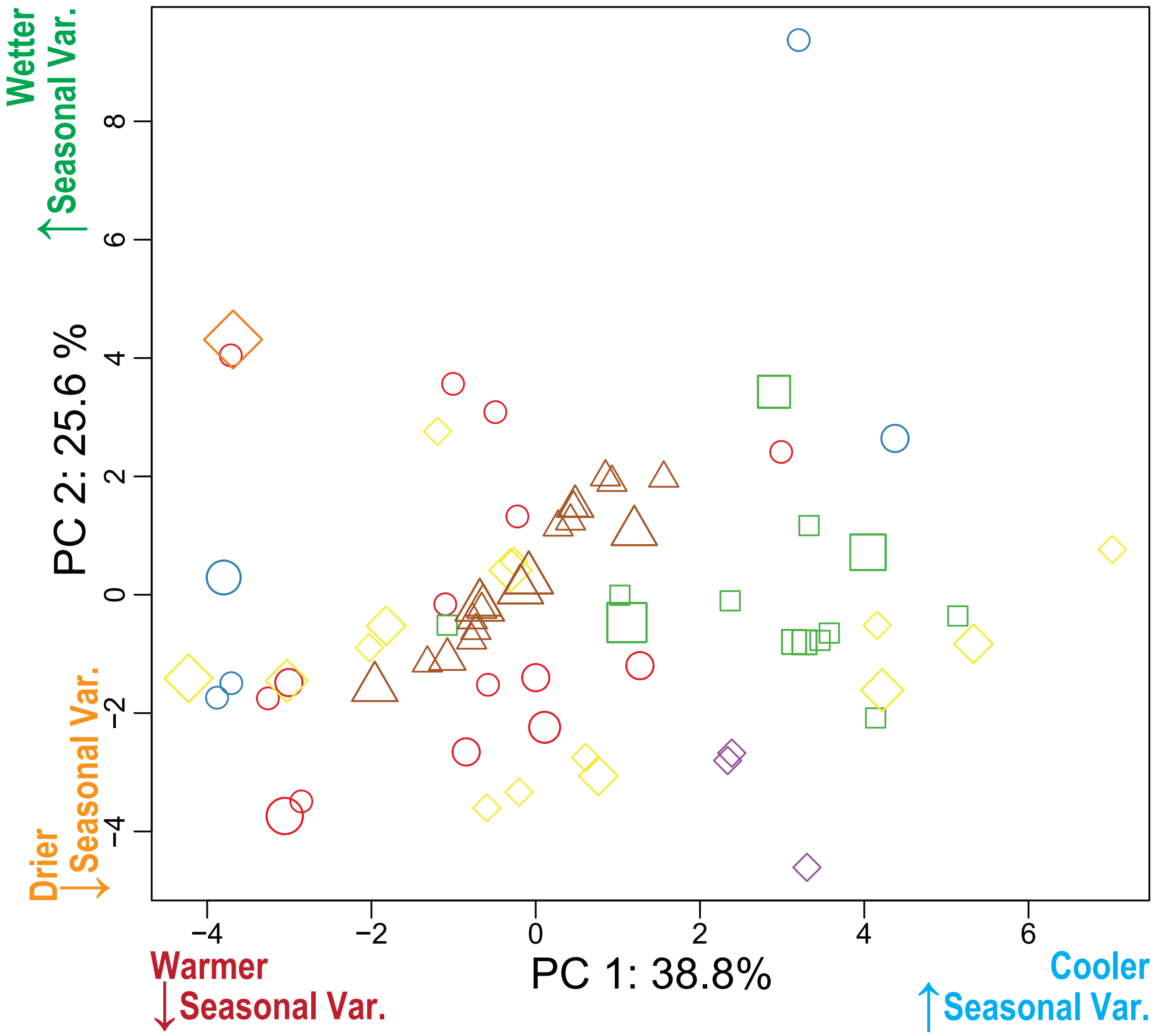

Manuscript body

Download source file (200.42 kB)

Tables

Table 1 - Download source file (18.44 kB)

Table 2 - Download source file (20.2 kB)

Figures

Figure 1 - Download source file (856.86 kB)

Figure 2 - Download source file (27.26 MB)

Figure 3 - Download source file (431.19 kB)

Figure 4 - Download source file (859.98 kB)

Figure 5 - Download source file (981.55 kB)

Figure 6 - Download source file (1.03 MB)

Figure 7 - Download source file (1.09 MB)

Figure 8 - Download source file (882.54 kB)

Supplementary Online Material

File 1 - Download source file (17.06 kB)

File 2 - Download source file (30.6 kB)

File 3 - Download source file (16.47 kB)

File 4 - Download source file (19.16 kB)

File 5 - Download source file (20.47 kB)

File 6 - Download source file (43 kB)

File 7 - Download source file (22.05 MB)

File 8 - Download source file (1.14 MB)

File 9 - Download source file (290.3 kB)